

Review

Applications of Laser Material Processing for Solid-State Lithium Batteries

Dongfang Yang 

National Research Council of Canada, London, ON N6G 4X8, Canada; dongfang.yang@nrc-cnrc.gc.ca

Abstract: Laser material processing is emerging as a critical manufacturing technology in the advancement of solid-state lithium batteries (SSLBs), offering numerous advantages in precision, efficiency, and versatility. This mini-review explores the applications and benefits of laser material-processing techniques, such as laser sintering, laser cutting, laser surface cleaning, laser ablation for nanoparticle generation, and pulsed laser deposition, in the fabrication and performance enhancement of SSLBs' materials and components. It will demonstrate that laser material processing can enhance material properties such as density and surface morphology, improve ionic conductivity and reduce interfacial resistance. Laser material-processing techniques are adaptable to a variety of materials, including polymers, metal oxides, metal sulfides, and metals, making them suitable for processing various SSLB components like electrolytes, electrodes, and current collectors. In addition, the use of laser material-processing technologies reduces manufacturing costs by minimizing material waste and streamlining production processes. Looking forward, integrating laser material processing with other advanced manufacturing technologies, such as roll-to-roll (R2R) manufacturing, for SSLBs holds promise for further scalability and efficiency. It is expected that laser material processing will be positioned to significantly contribute to the development of safer, more efficient, and cost-effective SSLBs, supporting their broader adoption across industries and paving the way for future innovations in energy storage technology.

Keywords: solid-state lithium batteries; laser material processing; laser ablation; laser sintering; laser cutting; laser surface cleaning; pulsed laser deposition; nanoparticles; solid electrolyte; impedance; anode; cathode



Academic Editor: Torsten Brezesinski

Received: 28 February 2025

Revised: 14 March 2025

Accepted: 18 March 2025

Published: 26 March 2025

Citation: Yang, D. Applications of Laser Material Processing for Solid-State Lithium Batteries. *Batteries* **2025**, *11*, 128. <https://doi.org/10.3390/batteries11040128>

Copyright: © 2025 by the author. Licensee MDPI, Basel, Switzerland. This article is an open access article distributed under the terms and conditions of the Creative Commons Attribution (CC BY) license (<https://creativecommons.org/licenses/by/4.0/>).

1. Introduction

The development of battery and energy storage technologies is key for the world's electrification, particularly for electric vehicles. Li-ion batteries have gained the most attention worldwide, with large investments made by governments and companies across the world. However, Li-ion batteries still have the challenges of relatively low energy density, slow charge rate, and flammability relating to the use of organic liquid electrolytes. Solid-state lithium batteries (SSLBs) that use metallic lithium for the anode and metal oxides or sulfides for the cathode potentially offer much higher cell voltage and energy density than that of lithium-ion batteries and, therefore, can boost the performance and extend the range of EVs. SSLBs are also cost-effective and have a wider operating temperature than conventional Li-ion batteries that use liquid electrolytes. The structure of an SSLB cell is schematically illustrated in Figure 1a. It consists of a cathode (or positive electrode), which can be a metal oxide or sulfide (e.g., LiCoO_2 , LiFePO_4 , NiS), a ceramic or solid polymer electrolyte (e.g., lithium lanthanum zirconium oxide (LLZO)) that also

works as the separator, an anode made of lithium metal (e.g., pure lithium or its alloys), and current collectors for the electrical contact with both the anode and the cathode (e.g., Al and Cu). The use of the solid electrolyte obstructs the growth of lithium dendrites at the anode/electrolyte interface and, therefore, allows the use of higher-energy-density lithium metal as the anode [1]. As the key component of SSLBs, the solid electrolyte plays a key role. It can offer improvement in the active material–electrolyte interface formation, cycling performance, and mechanical strength, since it eliminates the lithium-ion battery's interface issue, which results from side reactions occurring at the interface between the electrode materials and the liquid electrolytes. The reactions cause the formation of a passivation layer that increases the interfacial resistance and degrades battery performance. However, the challenges of using solid electrolytes, such as poor physical contact and mechanical stress, which create high interfacial resistance, need to be carefully mitigated. Solid electrolytes used in SSLBs include oxides, sulfides, phosphates, and solid polymers. The development of highly ionic conductive and stable electrolytes is the most critical requirement for advancing SSLB technology. Currently, LLZO, a garnet-type oxide material, has gained the most interest due to its high ionic conductivity, good chemical stability with lithium metal, and overall durability, making it a leading candidate for solid-state lithium metal batteries [2,3]. Lithium lanthanum titanate (LLTO), with a perovskite structure (i.e., ABO_3), has also gained a lot of attention due to its high bulk conductivity ($10^{-3} \text{ S cm}^{-1}$) at room temperature and its excellent chemical stability [4]. LLTO has many advantages, including negligible electronic conductivity, high voltage stability ($>8 \text{ V}$), and atmospheric and temperature stability. Higher ionic conductivity in the range of 10^{-4} to $10^{-2} \text{ S cm}^{-1}$ at room temperature was achieved by sulfide-based solid electrolytes, such as glassy sulfides represented by the binary systems, i.e., $\text{Li}_2\text{S}-\text{SiS}_2$, $\text{Li}_2\text{S}-\text{P}_2\text{S}_5$ and $\text{Li}_2\text{S}-\text{GeS}_2$, $\text{Li}_7\text{P}_3\text{S}_{11-x}$, and ternary systems by adding other compounds, such as Li_3N or LiI . In particular, $\text{Li}_7\text{P}_3\text{S}_{11-x}$ can reach $1.7 \times 10^{-2} \text{ S cm}^{-1}$ at room temperature after it has gone through thermal treatment optimization. As alternatives to those glassy sulfide solid electrolytes, $\text{Li}_{3+x}(\text{P}_{1-x}\text{M}_x)\text{S}_4$ ($\text{M} = \text{Si, Ge, Sn}$), $\text{Li}_{10}\text{MP}_2\text{S}_{12}$ ($\text{M} = \text{Si, Ge, Sn}$), and $\text{Li}_6\text{PS}_5\text{X}$ ($\text{X} = \text{Cl, Br}$) are also gaining increasing attention. However, sulfide-based solid electrolytes have limited chemical and electrochemical stability, resulting in narrow thermodynamic electrochemical stability windows [5]. Due to the characteristics of high ionic conductivity, excellent chemical stability with cathode materials, and a broad electrochemical potential window, halide materials, such as Li_3MCl_6 ($\text{M} = \text{In, Er, Sc, Ho, Y}$), have also become very attractive solid electrolyte candidates for SSLBs. However, many challenges, such as moisture sensitivity and anode interfacial instability, have to be overcome [6]. Other solid electrolytes that were investigated include lithium phosphorous oxynitride (LiPON) [7], lithium superionic conductor (LISICON) such as γ - Li_3PO_4 -type $\text{Li}_{3.75}\text{Ge}_{0.75}\text{P}_{0.25}\text{O}_4$ [8], other perovskites, etc.

SSLBs are intrinsically safe, since no liquid electrolyte is used. Therefore, it has great potential for a wide range of applications, including mobile devices, EVs, and grid storage. In addition, the miniaturization of SSLBs (i.e., micro batteries) by using thin-film deposition technologies allows their use in on-chip micro devices, portable/wearable devices, micro-electronics, and biomedical implants. SSLBs are expected to achieve significant market penetration and are currently the target of intense R&D activities worldwide. Research into low-cost and scalable manufacturing processes is crucial for enabling economic and industrial-scale production of SSLBs. The laser is an excellent material processing tool suited for manufacturing SSLBs. Examples of using a laser beam for the processing of SSLBs include laser sintering, laser nanoparticle generation, laser ablation surface cleaning, laser cutting, and pulsed laser deposition, which are schematically illustrated in Figure 1b.

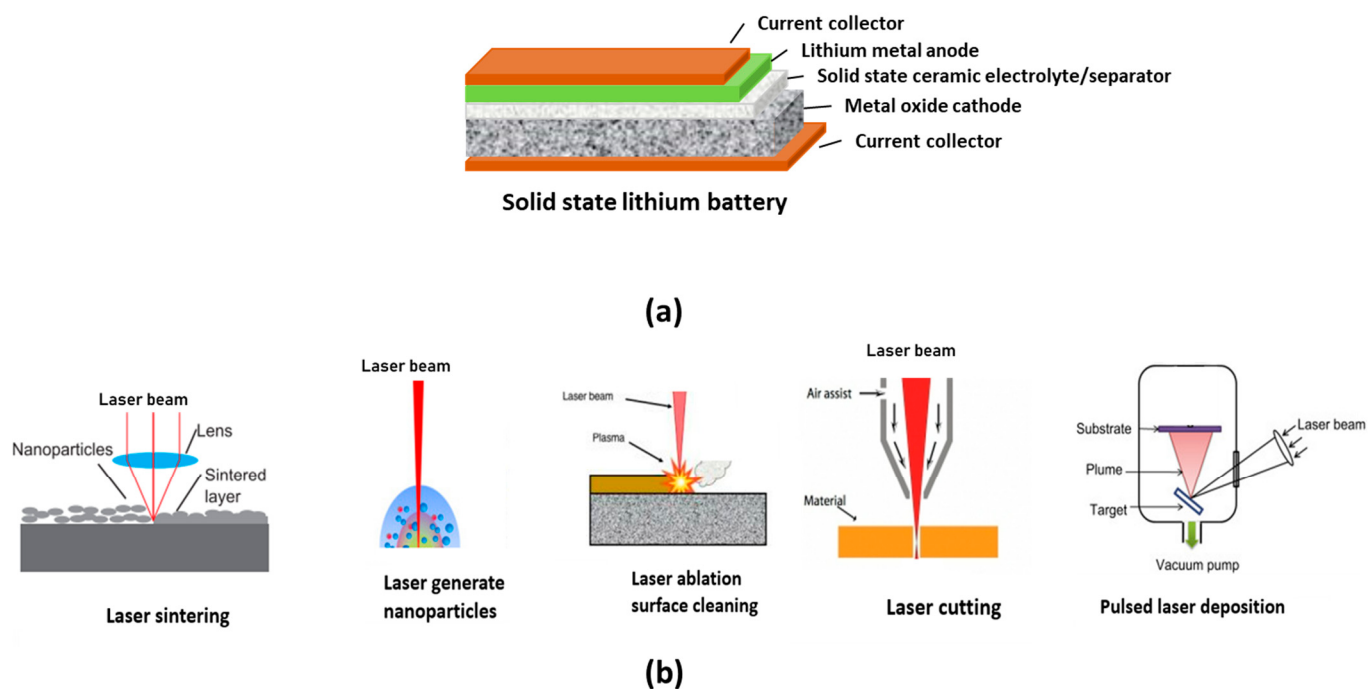


Figure 1. (a) The structure of a solid-state battery and (b) various laser processes used for SSLBs.

There are five main types of lasers, including gas lasers, solid-state lasers, fiber lasers, liquid lasers (i.e., dye lasers), and semiconductor lasers (i.e., laser diodes), that can be chosen for these applications to process SSLBs. A laser outputs either pulses or a continuous wave. Pulsed lasers can be classified as nanosecond, picosecond, and femtosecond lasers, depending on their pulse duration. Longer pulse lasers are generally more cost-effective than shorter pulse lasers, while shorter pulse lasers generally improve machining quality and the material removal rate. A pulsed laser can produce peak power greater than its average power. Therefore, it is a very efficient energy source for spot welding and seam sealing of battery tabs for single cells when a small heat-affected zone is needed. In contrast, continuous-wave lasers can generate heat that penetrates deep into materials at high processing speeds and are a good option for the high-speed seam welding of battery tabs to terminals. The choice of a laser for processing SSLBs depends on the material/components being machined, the desired machining quality, and the cost. Nanosecond lasers have high ablation efficiency, making them suitable for the evaporation and deposition of thin films for SSLBs' cathode and solid electrolyte, while femtosecond lasers can enable cold processing of materials, providing high surface finishing, and are suitable for the micromachining and patterning of SSLBs' solid electrolyte and cathode components. Picosecond lasers have a relatively high ablation rate and can be effective at controlling the heat-affected zone in metal machining, which are suitable for micro-machining Li anode and current collectors.

The primary wavelengths for lasers include the ultraviolet, visible, and infrared regions of the light spectrum. Ultraviolet lasers consist of wavelengths between 180 and 400 nanometers (nm), while visible lasers consist of radiation with wavelengths between 400 and 700 nm. The infrared lasers cover wavelengths between 700 nm and 1 mm. Laser wavelength is a critical factor that significantly impacts the laser material processing. Laser wavelengths determine how lasers interact with different materials, affecting absorption, penetration, and precision. The ultraviolet wavelength is short, and therefore, material processing can achieve better precision and accuracy. Since most materials absorb light strongly at the ultraviolet wavelength range, therefore, ultraviolet lasers are best for surface cleaning, as well as for the evaporation and deposition of thin films. An infrared wavelength

can penetrate the materials, enhancing absorption. As a result, the material surface heats up, leading to vaporization, making infrared lasers a popular choice for cutting. However, their higher reflectivity can pose challenges in some applications.

The main advantage of using laser material processing for SSLBs is the ability to process all of the SSLBs' components, including metallic current collectors, the Li metal anode, the metal oxide or sulfide cathode, and the ceramic and polymer solid electrolytes. This can be conducted by simply adjusting the laser's parameters, such as peak power, wavelength, and pulse duration. Laser material processing is a non-contact technique, which prevents contamination of the SSLBs' materials and components. In addition, the laser process can be easily automated thanks to its high speed, high accuracy, and repeatability. The laser process can machine very small features down to the micron level, allowing for the interfacial engineering of SSLBs in the microscale. Laser processing has replaced a variety of traditional material-processing applications, such as cutting and welding, in manufacturing batteries. The use of laser energy to process SSLBs has made tremendous progress and is now at the forefront of battery-manufacturing applications.

This mini-review describes recent advances in using lasers to process materials and components for SSLBs. The laser process technologies presented in this review include (i) laser annealing/sintering; (ii) laser nanoparticle generation; (iii) laser ablation surface cleaning, (iv) laser cutting; (v) other laser machining processes such as interfacial engineering and drilling; and (vi) pulsed laser deposition. The mini-review will demonstrate that using lasers for the processing of SSLBs can give rise to high performance hard to achieve by other conventional materials processing.

2. Laser Ablation and Machining of Materials and Components in SSLBs

Laser material processing involves using high-energy laser beams to sinter, modify, or precisely remove material from a surface. The technology can be used to modify surface properties to improve adhesion, roughness, microstructures, phases, and wettability and to create intricate patterns and structures, which are required in SSLB materials and components. The technology plays a crucial role in optimizing interfaces between solid electrolytes and electrodes, reducing interfacial resistance and enhancing ionic conductivity. Laser material-processing technologies are increasingly being explored for the fabrication and enhancement of SSLBs, offering significant advantages in precision, efficiency, and material versatility. The roles and benefits of the laser material-processing technology will be illustrated in the following examples.

2.1. Laser Sintering

Producing a metal oxide solid electrolyte plate by traditional sintering techniques, such as solid-state sintering, requires several hours of processing of the metal oxide powder at a high temperature but below its melting point. Although those processes have been proven to yield desirable crystal structures, the low ionic conductivity of metal oxide solid electrolytes after sintering that resulted from inferior microstructure and lithium loss is still a significant challenge. In addition, due to their intrinsic brittleness and air sensitivity, the fabrication of high-performance metal oxide solid electrolytes for SSLBs remains highly difficult.

Laser annealing/sintering uses a laser beam to heat the surface or a specific area of a metal oxide solid electrolyte plate locally, followed by rapid cooling to modify its properties, such as density and crystal structures. Laser annealing/sintering allows for heating only the surface while not damaging the underneath structure, which is very useful for the direct fabrication of a metal oxide solid electrolyte layer over the cathode or anode in an SSLB cell. Additionally, the depth of the sintered layer can be controlled by selecting the

laser parameters, such as wavelength, pulse duration, and energy. For example, ultraviolet lasers having a short absorption depth are suitable for heat treatment of only the top surface layer of the oxide solid electrolyte to modify its properties and facilitate the deposition of the cathode active materials. The infrared laser can penetrate deeply into the materials, enhancing the sintering of thick cathode and electrolyte layers.

In SSLBs, it is necessary to mix the cathode active material particles with the highly Li^+ conductive solid electrolyte particles to generate a hybrid cathode with a high ionic conductivity, since the ionic conductivity of the cathode material itself is usually not high enough. Mixed particles of cathode active material and electrolyte must be sintered to form a dense layer so that it will function properly. Since the laser sintering process enables short interaction times at elevated temperatures, diffusion between active materials and electrolytes and the formation of unwanted phases could be reduced. L. C. Hoff et al. [9] investigated the use of the laser sintering method to treat the surface of a screen-printed mixed cathode layer in an SSLB cell to achieve higher ionic conductivity. The multilayer SSLB cell used in their study is schematically shown in Figure 2. A thin metallic substrate made of steel is used as the current collector. On top of it, a mixed cathode layer, a $\text{Li}_7\text{La}_3\text{Zr}_2\text{O}_{12}$ (LLZO) solid electrolyte layer, and a Li anode layer were deposited subsequently by screen printing from their pastes. The cathode layer consists of a mixture of cathode active material (e.g., lithium cobalt oxide (LCO) or lithium nickel manganese cobalt oxide (NMC)) and the solid electrolyte LLZO.

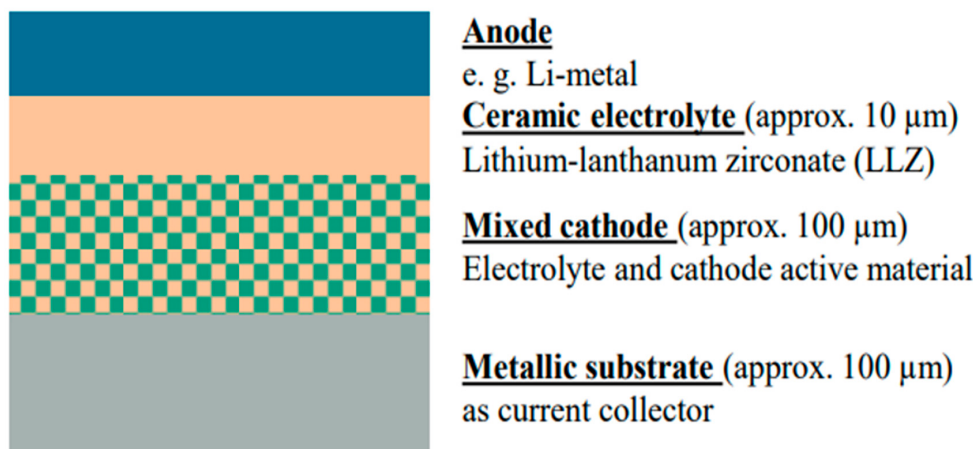


Figure 2. A solid-state battery layer structure. Reproduced from [9], copyrighted of SPIE.

The multilayer SSLB cell was thermally treated and sintered to achieve good interfacial contacts. Since conventional oven sintering (Figure 3 left) needs long interaction times (in the range of minutes), it leads to element diffusion between the materials and induces their crystal structure changes, resulting in undesirable phases. Laser sintering (Figure 3 right) that uses laser radiation to heat and melt particles is characterized by short interaction times in the sub-second range. Due to the shorter interaction times, the diffusion between particles is limited. Therefore, the crystal structure of the particles can be maintained. In addition to oven and laser sintering, rapid thermal processing (RTP) using light to heat and sinter (in seconds to minutes) was also used by the authors for comparison.

An infrared laser with a wavelength of 1470 nm and a maximum laser power of 250 W was used by the authors to scan the surface of the mixed cathode at a selected speed with the help of a two-axis motion system (Figure 4a). The infrared wavelength was used because it can penetrate deeply into the materials, enhancing the sintering of the mixed cathode. Figure 4b shows the XRD diffraction patterns of an untreated, laser-sintered, and RTP-processed mixed cathode. The XRD patterns show an increase of undesired lanthanum

cobalt oxide (LaCoO_3) phases and a decrease in LCO and LLZO phases for all the sintered mixed cathode layers compared to the untreated one. However, the laser-sintered mixed cathode layer shows a lower percentage of the unwanted LaCoO_3 phase than that of the RTP-treated cathode layer. The results demonstrated that the laser-sintering process is best for the preservation of desired crystal phases for LLZO and LCO, which is important for maintaining the good electrochemical properties of the SSLB.

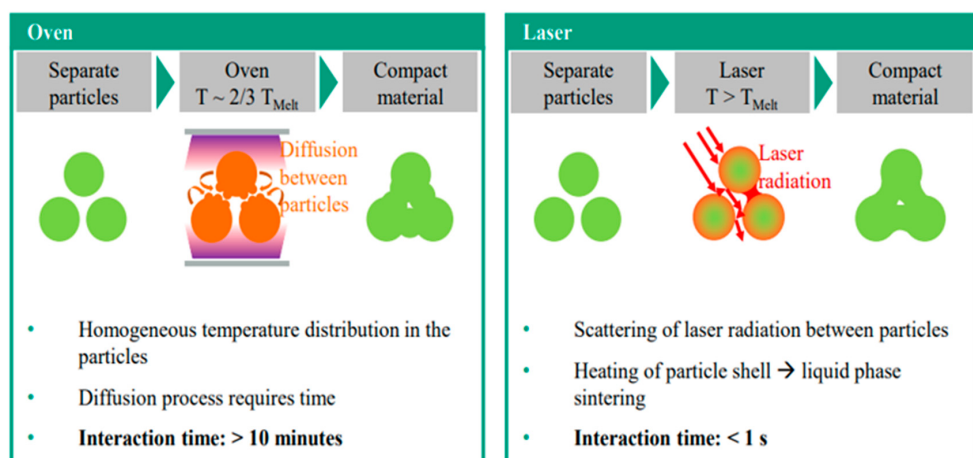


Figure 3. A comparison of oven sintering and laser sintering. Reproduced from [9], copyright of SPIE.

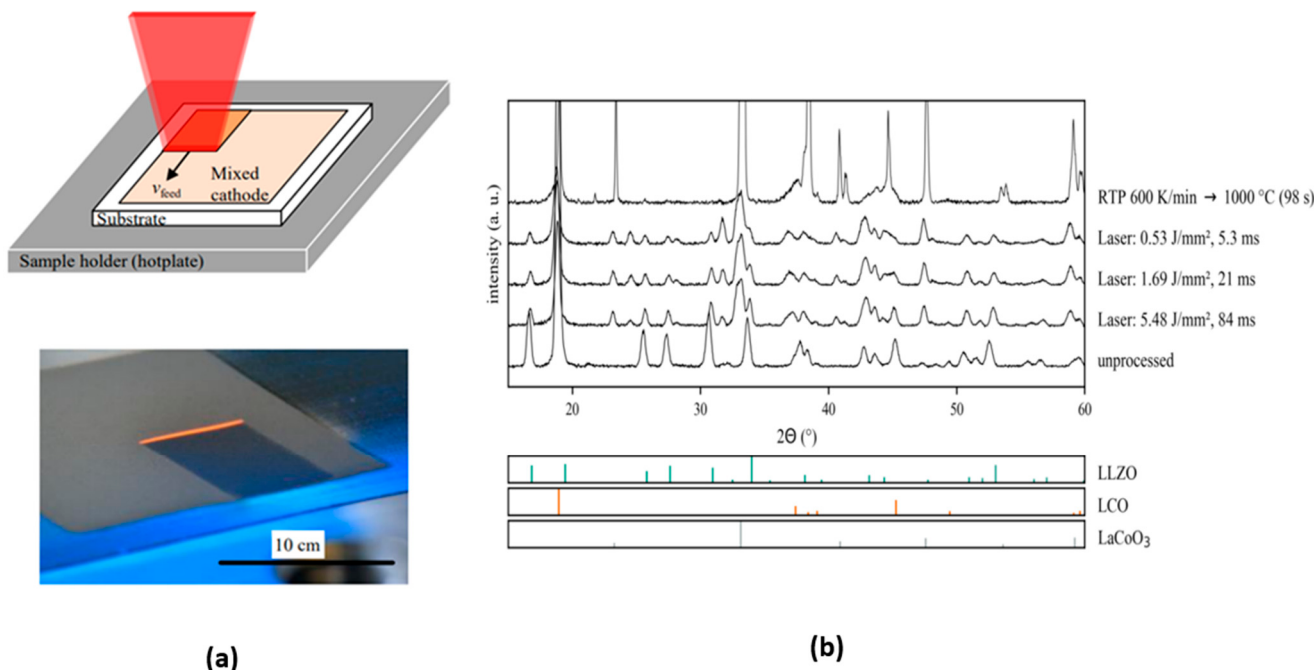


Figure 4. (a) Experimental set-up and picture for laser-sintering process; (b) XRD patterns of untreated, laser-sintered, and rapid thermal-processing-treated mixed cathode layers. Adapted from [9], copyright of SPIE.

Recently, A. Santomauro et al. [10] also used a laser rapid reactive sintering method to prepare fully dense $\text{Li}_7\text{La}_3\text{Zr}_2\text{O}_{12}$ -based solid oxide electrolytes. By optimization of the laser parameters, electrolyte precursor composition, and controlled atmospheres, they were able to produce solid oxide electrolytes with low lithium element loss, a desired crystal phase/microstructure, and high ionic conductivity. A. Hasani et al. [11] used a reactive laser-sintering process to generate high density and low Li loss and pure

LLZO phase solid electrolyte with various grain structures that allow them to optimize the ion transport properties of the LLZO and its interface with active materials. H. Wehbe et al. [12] investigated the effects of laser pulse frequency and pulse width of an infrared laser with a wavelength of 1062 ± 3 nm on the topology and morphology of the laser-sintered NASICON-type, $\text{Li}_{1+x}\text{Al}_x\text{Ti}_{2-x}(\text{PO}_4)_3$, solid electrolyte pellets. They found that the arithmetic surface roughness and depth of the sintered layer of the pellets were the key factors that affected the properties of the electrolyte. Other works reporting the laser sintering of solid electrolytes include P. Kaya et al. [13], who sintered $\text{Li}_{6.6}\text{La}_3\text{Zr}_{1.6}\text{Ta}_{0.4}\text{O}_{12}$ (LLZTO) with near-infrared and middle-infrared lasers at varying process parameters, such as laser power, scan speed, and track overlap, to optimize the sintering process of a solid electrolyte for solid-state batteries. G. Ryoo et al. [14] used an infrared laser of short and ultrashort laser pulses to sinter ceramic solid electrolyte $\text{Li}_{1+x}\text{Al}_x\text{Ti}_{2-x}(\text{PO}_4)_3$ and then used scanning electron microscopy to analyze its surface quality to understand the melt formation at high fluences with pulse bursts.

In summary, the laser sintering of powders of a metal oxide solid electrolyte or cathode or their mixtures offers advantages such as short processing time to avoid interdiffusion of constituent materials. In addition, by adjusting the laser parameters and powder characteristics, it is possible to tailor the properties of the sintered ceramic solid electrolytes and cathodes. However, rapid heating and cooling during laser sintering can introduce internal thermal stresses, potentially leading to cracks in the final SSLBs' components. Also, due to the high temperatures involved in the sintering process, components of SSLBs can experience shrinkage during cooling, leading to potential dimensional inaccuracies.

2.2. Laser Generates Solid Electrolyte Nanoparticles

Polymer-based solid-state electrolytes are an alternative to metal oxide electrolytes for SSLBs. Poly(ethylene oxide) (PEO)-based solid-state electrolytes have the benefit of low cost, non-flammability, and can block Li dendrite formation and growth, thus offering a great benefit for SSLBs. However, the tendency of PEO to form a crystalline phase obstructs its Li^+ migration and, thus, reduces its Li^+ ionic conductivity. Various approaches, such as adding ion-conductive metal oxide particles, to promote the formation of amorphous phase in various regions were exploited. Among these methods, incorporating Li conductive metal oxide particles into the PEO matrix has been recognized as one of the helpful ways to improve its ionic conductivity, mechanical properties, and interfacial stability. For example, adding 10 wt% bulk LLZTO into the PEO electrolyte membrane caused a conductivity enhancement of up to an order of magnitude [15]. Reducing the particle size of the metal oxide particles from the microscale to the nanoscale could further provide a higher surface area, which allows for increased interfacial contact with the PEO, thereafter increasing the Li^+ ion conduction pathways [16]. Laser ablation for nanoparticle synthesis uses a laser beam with a high pulse energy and short pulse duration, such as a KrF excimer laser to irradiate and vaporize material from its surface, which then rapidly cools and condenses, forming nanoparticles with controlled sizes and compositions. This method can be conducted in vacuum, gas, or liquid environments, offering versatility in producing various nanoparticles. Compared to laser sintering, which uses a laser beam to heat and bond particles without fully melting them, laser ablation involves the removal of material from its surface through heating and vaporization. Y. Su et al. [17] reported the use of a liquid-phase laser ablation process to in situ generate nanoscale $\text{Li}_{6.4}\text{La}_3\text{Zr}_{1.4}\text{Ta}_{0.6}\text{O}_{12}$ particles (Nano-LLZTO). In their works, large LLZTO particles (Bulk-LLZTO) were dispersed into the polyethylene glycol (PEG)/acetonitrile (ACN) solution by ultrasonication. Then, the mixed dispersion was irradiated with a Nd: YAG laser (pulse width of 10 ns, repetition rate of 30 Hz, and laser fluence of $152 \text{ mJ pulse}^{-1} \text{ cm}^{-2}$) with a wavelength of 355 nm,

as shown in the schematic diagram in Figure 5a. The use of the third harmonic generation, 355 nm wavelength, of Nd:YAG lasers (1064 nm) is to allow for more light-energy absorption by LLZTO particles, which is beneficial for nanoscale particle formation. After laser irradiation, the authors found that the Bulk-LLZTO was converted into spherical nanoparticles with a uniform particle size distribution (Figure 5c). From the high-resolution TEM image (Figure 5d), the lattice spacing of 0.26 nm was determined, corresponding to the interplanar d-spacing of the (422) plane of LLZTO. Based on the TEM image, they determined that the average size of Nano-LLZTO is ~8.3 nm. The chemical composition of LLZTO was also analyzed by the energy-dispersive X-ray spectroscopy elemental mappings (Figure 5e), which show the homogeneous distributions of La, Zr, Ta, and O over LLZTO particles. The XRD pattern of Nano-LLZTO is shown in Figure 5f. The characteristic peaks of Nano-LLZTO are almost essentially as those of pristine LLZTO (JCPDS: 80–0457), revealing that the laser irradiation does not induce a change in the crystal structure of LLZTO. The composite electrolyte that consists of PEO and PEG-coated Nano-LLZTO was prepared by the solvent-casting procedure, accompanied by hot pressing. The as-obtained electrolyte was named as Nano-LLZTO CSE.

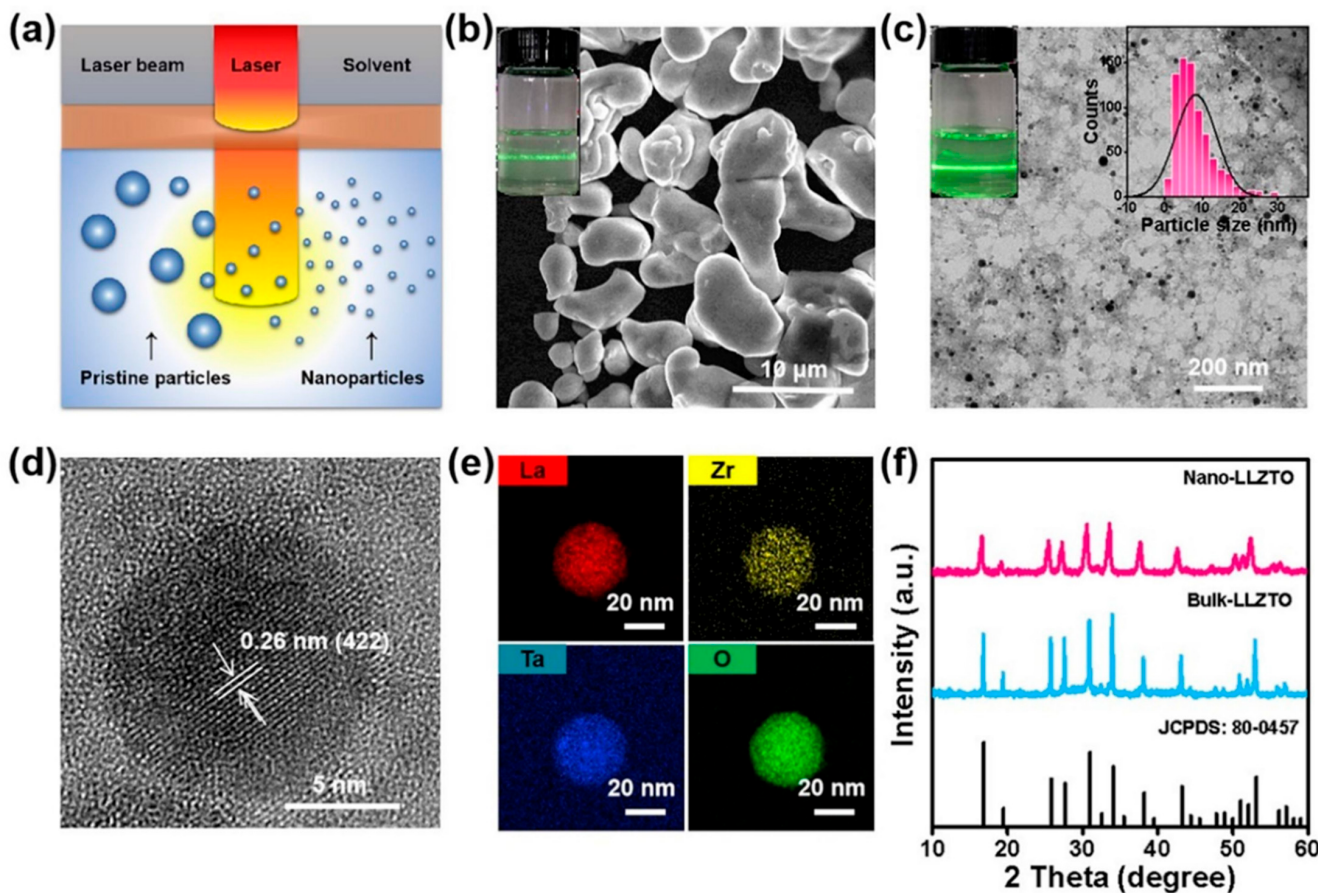


Figure 5. LLZTO before and after laser irradiation, (a) The schematic diagram of the laser irradiation process. (b) The SEM image of the LLZTO before laser irradiation. (c) The TEM image of laser-irradiated LLZTO. (d) The HRTEM image of laser-irradiated LLZTO, (e) The corresponding elemental mappings of La, Zr, Ta, and O of laser-irradiated Nano-LLZTO colloids in the presence of PEG. (f) XRD patterns of the LLZTO before and after laser irradiation (in the absence of PEG). The inset in Figure 6b is the digital photo of the LLZTO suspension before irradiation. The insets in Figure 5c are the digital photo and a size distribution histogram of Nano-LLZTO suspension after irradiation. Reproduced with permission [17], copyright of Elsevier.

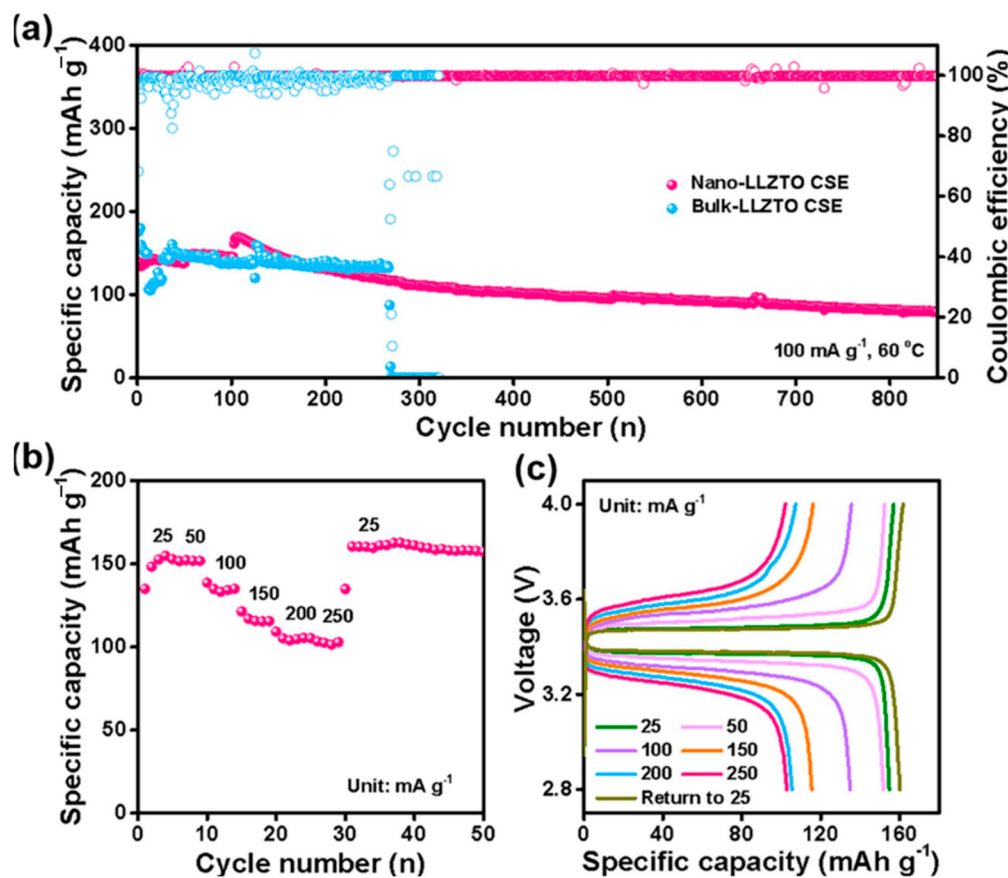


Figure 6. (a) Cycling performance of LFP | Nano-LLZTO CSE | Li and LFP | Bulk-LLZTO CSE | Li at 100 mA g^{-1} at 60°C . (b) The rate performances of LFP | Nano-LLZTO CSE | Li at 60°C . (c) Charge-discharge voltage profiles of LFP | Nano-LLZTO CSE | Li at different current densities. Reproduced with permission [17], copyright of Elsevier.

The LLZTO-filled PEO electrolyte was evaluated by the authors in full cells inside of which LiFePO₄ (LFP) is used as a cathode and Li metal as an anode. The LFP | Nano-LLZTO CSE | Li cell exhibits the initial charge and discharge capacity of 144.5 and 136.4 mAh g^{-1} at a current density of 100 mA g^{-1} at 60°C , respectively, correlated to the initial coulombic efficiency of 94.4%. After the cell was cycled for more than 850 cycles, a capacity retaining of 58.5% was obtained (Figure 6a). For comparison, the full cell with large LLZTO particles, i.e., LFP | Bulk-LLZTO CSE | Li, only lasted for 250 cycles. Its specific capacity reduced suddenly to zero due to the short circuit by the Li dendrite penetration, as suggested by the authors. Figure 6b,c display the cycling performance of an LFP | Nano-LLZTO CSE | Li battery under various current densities at 60°C . Specific capacities of 154.8, 151.7, 135.0, 115.5, 105.4, and 102.8 mAh g^{-1} were obtained at current densities of 25, 50, 100, 150, 200 and 250 mA g^{-1} , respectively. When the current density was switched back from 250 to 25 mA g^{-1} again, the discharge-specific capacity was restored to 162.5 mAh g^{-1} , which is indicative of the high electrochemical stability of Nano-LLZTO CSE. The results of Y. Su et al. show that laser ablation is capable of producing nanosized high-purity LLZTO particles that maintain the crystal structure and chemical composition of the LLZTO bulk material. This work by Y. Su et al. also demonstrated that incorporating metal oxide ion conductor nanoparticles into a Li⁺ conductive polymer matrix is an efficient strategy for developing hybrid solid-state electrolytes with high ionic conductivity for SSLBs.

Y. Su et al. [18] also used an Nd: YAG laser with the third harmonic generation wavelength of 355 nm (repetition rate of 10 Hz, pulse width of 10 ns) to prepare nanosized TiO₂ and then coated the TiO₂ nanoparticles with poly acetonitrile. Due to the strong

absorption at the 355 nm ultraviolet wavelength of the laser radiation by TiO_2 , a 13 nm average size of TiO_2 nanoparticles was obtained. The nanosized TiO_2 was then used as fillers for the PEO polymer electrolyte. The hybrid electrolytes show combining benefits of high ionic conductivity, high Li^+ transference number, superior electrochemical stability, and enhanced mechanical robustness. A lithium symmetric battery with nanosized TiO_2 -PEO composite solid electrolytes exhibits a stable cycling life of up to 590 h at 0.25 mA cm^{-2} . The full Li metal batteries with a LiFePO_4 cathode deliver superior durability for 550 cycles.

In summary, laser ablation offers advantages, like producing high-purity nanoparticles, since the nanoparticles are directly ablated from a target material. As compared to nanoparticles synthesized by chemical solution methods, laser ablation minimizes contamination from chemical reactions. In addition, due to the strong absorption of laser beams at the ultraviolet wavelength range by almost all materials, a variety of materials can be used as targets, allowing for the fabrication of a wide range of nanoparticle compositions. Also, by adjusting laser parameters like wavelength, pulse duration, power, and repetition rate, some degree of control over the size of the produced nanoparticles can be achieved. However, there are limitations of the laser ablation for nanoparticle production, including that (i) the production rate is relatively low, making it impractical for large-scale synthesis; (ii) nanoparticles produced by laser ablation can tend to agglomerate, requiring additional stabilization techniques; and (iii) precise control of the laser parameters is crucial for achieving desired nanoparticle properties, which can be complex and time-consuming.

2.3. Laser Ablation Surface Cleaning

Surface contamination in SSLBs can be a substantial problem that compromises their performance, efficiency, and longevity. Conventional methods like sandblasting, manual scrubbing, chemical etching, or ultrasonic cleaning are slow, expensive, and can damage SSLBs. Laser surface cleaning, however, provides an efficient and resilient solution, easily tailorabile to different materials and components. Laser surface cleaning is based on the laser ablation process to remove a material layer or a coating. During the process, high-energy laser radiation was absorbed by the atoms of a surface layer, causing the breakdown of the chemical bonds to form rapidly expanding plasma. The plasma can also generate shock waves that help remove the surface layer from the substrate. Compared to traditional surface-cleaning methods, a laser surface-cleaning process possesses several unique advantages, such as (1) being environmentally friendly; (2) having a wide range of surface contaminants that can be removed from various substrates; (3) causing limited damage to the substrate by properly adjusting the laser-processing parameters; (4) having no mechanical contact to the substrate surface; and (5) fast processing that is easy to automate.

Laser surface cleaning can remove surface contamination for SSLBs during their production, which significantly increases their quality and performance. Surface contamination can often lead to defects, short circuits, or leakages, either of which can have negative impacts on the SSLBs. For example, garnet-type solid electrolyte LLZTO reacts to CO_2 and H_2O in the air to form a Li_2CO_3 insulating layer on its surface, leading to poor interface contact and large interfacial resistance with the Li anode. Formation of the Li_2CO_3 insulating layer also induces fast Li dendrite growth and propagation through the electrolyte attributable to the locally high current density. This can cause short circuits and thermal runaway. L. Chen et al. [19] introduced the laser ablation surface-cleaning method to effectively remove the Li_2CO_3 layer from the garnet electrolyte surface, resulting in a clean surface that affiliates with lithium. The laser-cleaning method that they used is schematically shown in Figure 7a,b. The LLZTO pellet was irradiated by a Nd:YAG laser operating at the second harmonic generation wavelength of 532 nm and 10 ns pulse

duration at a frequency of 30 kHz. The use of an ultraviolet laser wavelength of 533 nm allows for more light energy absorption by the LLZTO surface, which is beneficial for laser ablation surface cleaning. To diminish the surface ablation and cut off the moist air, the garnet pellet was covered with a small amount of a 5% PEO–acetonitrile solution during line-by-line laser scan cleaning by the authors. The effect of laser processing was controlled by adjusting the power and scanning rate, achieving different spot overlap ratio.

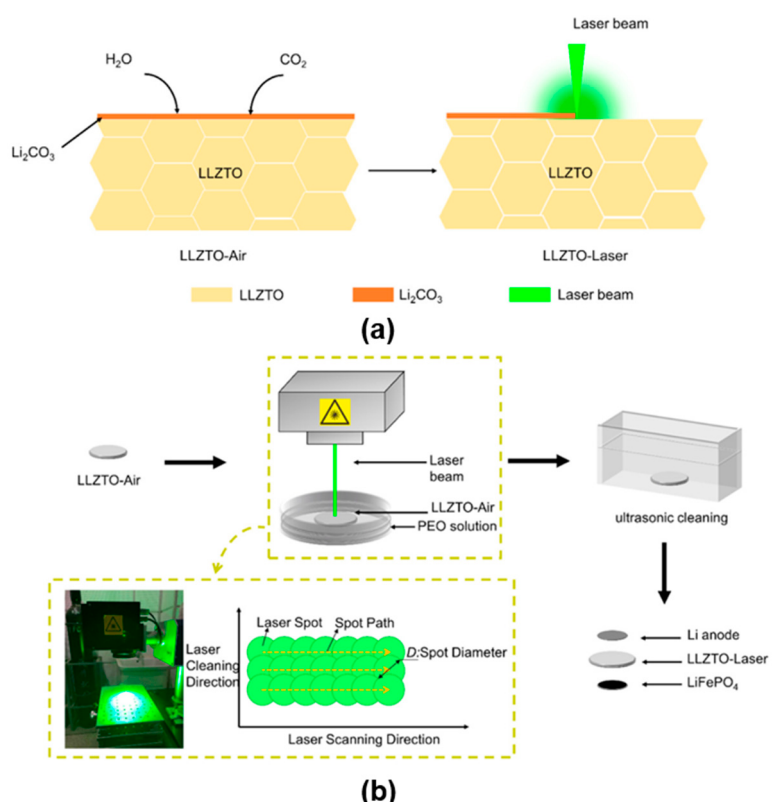


Figure 7. Schematic illustration of (a) Li_2CO_3 formation on LLZTO and the laser-cleaning process and (b) step-by-step of the laser-cleaning process on the garnet surface. Adopted with permission from [19], copyright of American Chemical Society.

The laser-cleaned LLZTO was evaluated by the authors in SSLB cells assembled with either untreated LLZTO (LLZTO-air) or laser surface-cleaned LLZTO (LLZTO-Laser). The SSLB cells used Li metal as the anode and the LiFePO₄ (LFP) composite as the cathode. The total impedance of the Li/LLZTO-Laser/LFP cell, which is 1760Ω , is much smaller than that of the Li/LLZTO-Air/LFP cell, as shown in Figure 8a, due to the reduced Li/LLZTO interfacial resistance. The Li/LLZTO-Laser/LiFePO₄ cell displayed small polarization and smoother voltage plateaus with a 2.8–3.8 V cutoff voltage window (Figure 8b). The charge–discharge voltage profiles of Li/LLZTO-Laser/LiFePO₄ at different C rates are shown in Figure 8c. The discharge capacities of the full cell were 149.6, 134.3, and $103.6 \text{ mA h} \cdot \text{g}^{-1}$ at 0.1, 0.2, and 0.5 C rate, respectively (Figure 8d). The discharge capacity regained to a almost identical level ($129 \text{ mA h} \cdot \text{g}^{-1}$) when the rate restored to a 0.1 C rate. The battery produced an initial specific discharge capacity of $149.3 \text{ mA h} \cdot \text{g}^{-1}$ and a Coulombic efficiency of ~100% at 0.1 C and 40 °C (Figure 8e). The Li/LLZTO-Laser/LiFePO₄ cell sustained a capacity retention of 98.9% at the 50th cycle, demonstrating excellent cycling performance. The discharge capacity gradually dropped to $126.6 \text{ mA h} \cdot \text{g}^{-1}$, with a capacity retention of 84.8% after 100 cycles. The high capacity and good cycling performance were credited by the authors to the fast and uniform Li^+ transport across the garnet/Li interface after laser surface cleaning of the LLZTO electrolyte. The capacity drops at the 50th~100th cycle was

assigned to the irreversible volume evolution of the Li anode and LiFePO₄ during long cycling.

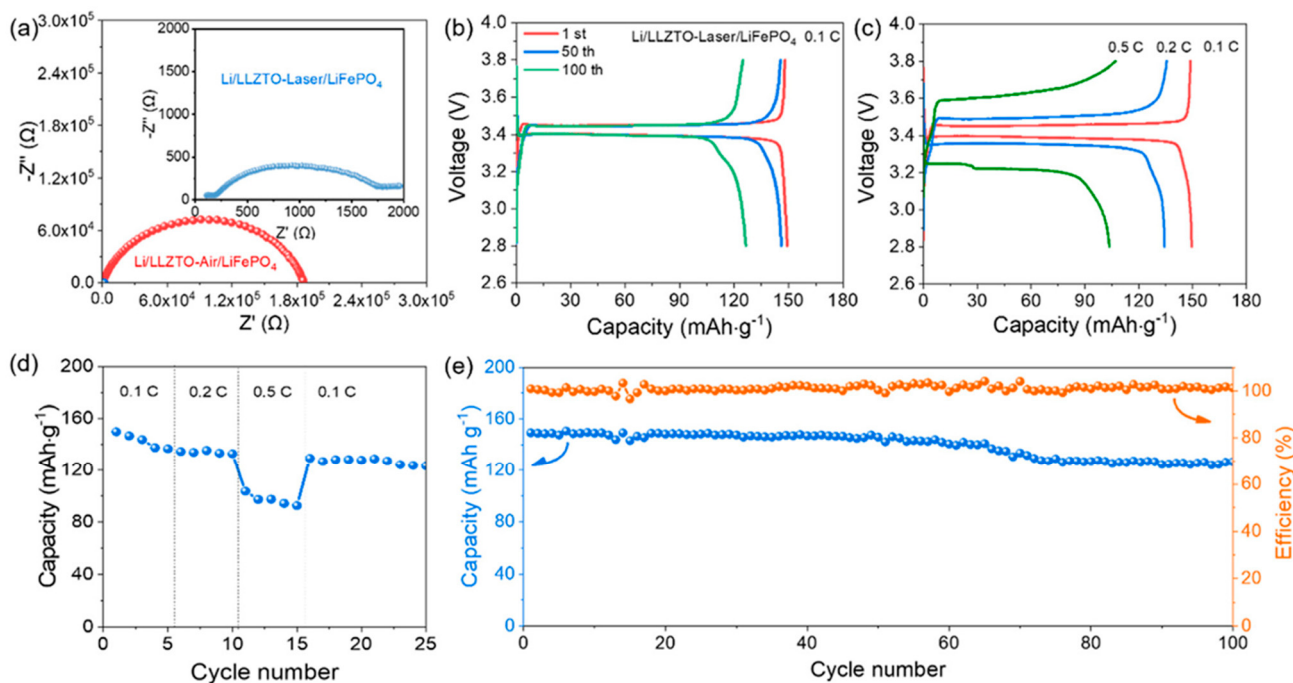


Figure 8. (a) EIS patterns of Li/LLZTO-Laser/LiFePO₄ and Li/LLZTO-Air/LiFePO₄ at 40 °C. The inset presented the enlarged EIS pattern of the Li/LLZTO-Laser/LiFePO₄ cell. (b) Charge–discharge curves of the Li/LLZTO-Laser/LiFePO₄ cell at 0.1 C and 40 °C. (c) Charge–discharge curves of Li/LLZTO-Laser/LiFePO₄ cell at 0.1, 0.2, and 0.5 C. (d) Rate performance (at 0.1, 0.2, and 0.5 C) and (e) cycle performance of the Li/LLZTO-Laser/LiFePO₄ cell at 40 °C. Reproduced with permission [19], copyright of American Chemical Society.

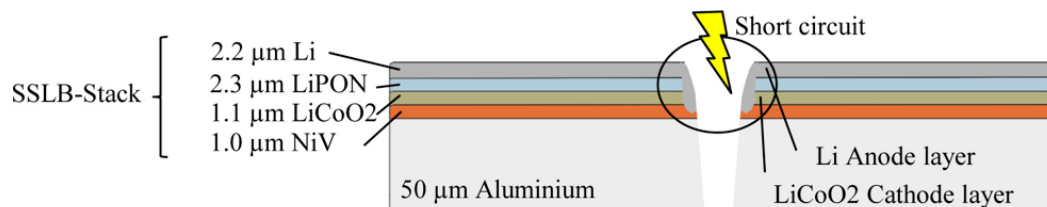
Laser surface cleaning can also be used to clean battery cell tabs and busbars to eliminate organic and inorganic impurities from surfaces before welding to ensure strong electrical connections between cells. In this aspect, established methods such as ultrasonic, chemical, and plasma cleaning techniques often be lacking in terms of performance or feasibility. However, laser surface cleaning works best on thin coatings, and thicker layers may require multiple passes, increasing the cleaning time and reducing productivity. In addition, localized heating induced by the high-energy laser beam during surface cleaning can sometimes cause thermal stress and lead to micro-cracks, phase changes, or degradation of the underneath solid electrolyte. Also, during laser surface cleaning, the interaction of laser energy with the solid electrolyte surface might result in chemical changes, potentially altering the stoichiometry or creating unwanted reaction products. Those damages can negatively affect the mechanical stability and ionic conductivity of the electrolyte and affect its performance and long-term stability. In addition, not all solid electrolyte materials respond well to laser cleaning. Some may be more prone to damage or degradation, requiring careful tuning of the laser's wavelength, pulse duration, and energy density to avoid adverse effects.

2.4. Laser Cutting

As a non-contact machining process, laser cutting will be one of the key steps in the production of SSLBs. Laser cutting works by directing a high-power laser beam to irradiate the workpiece to melt, burn, and vaporize away materials, resulting in a cut edge. Laser cutting is a high-speed and accurate process compared to other cutting methods, such as plasma, or blade cutting. Laser-cutting technology offers a highly flexible method to cut

single cells of SSLB rolls that are produced by the R2R manufacturing process. Laser-cutting technology is essential for producing large quantities of SSLB cells, since other methods, such as blade-cutting and punching processes, easily cause short-circuiting between the layers of SSLBs. C. Hördemann [20] employed an ultra-short pulsed laser-cutting method to dice flexible SSLBs with the structure Al/NiV/LiCoO₂/LiPON/Li, as schematically illustrated in Figure 9. Conventional cutting of SSLBs using a continuous laser or knife is also shown in the figure for comparison. In the figure, the respective thicknesses of the layers in the battery stack are shown. The aluminum substrate is covered by a NiV current collector that also acts as a diffusion barrier between the aluminum substrate and the cathode. The cathode material is LiCoO₂, and the anode is composed of lithium, which is deposited via evaporation deposition. Through selective ablation of the individual layers, contact areas or functional sections can be created via ultrashort pulsed laser ablation. This allows for attaching contact taps to the electrodes and also prevents the battery from failing due to short circuits between layers while cutting. Mechanisms for the ultrashort pulsed laser ablation of thin layers can be very different depending on the material of the layer, its substrate, and the laser's parameters (i.e., pulse duration, laser power, and wavelength). These ablation mechanisms can be classified as photochemical ablation, photothermal ablation, photomechanical ablation, and blast-off ablation [20]. Photochemical ablation is mainly observed while ablating organic material, where laser radiation in the UV range to break chemical bonds is mostly used. Photothermal ablation takes place if the energy threshold for the ionization of the material is not reached and the material is heated and evaporated. Photomechanical ablation is induced due to the stress between the substrate and the layer. Blast-off ablation can be noticed if the thin layer has low absorption of laser radiation but abundant photons are absorbed in the substrate.

Conventional cutting (cw-laser/knife) can lead to short circuits when anode and cathode layer get in contact melt or residues



After ablation of electrodes contact areas and region for cutting are prepared

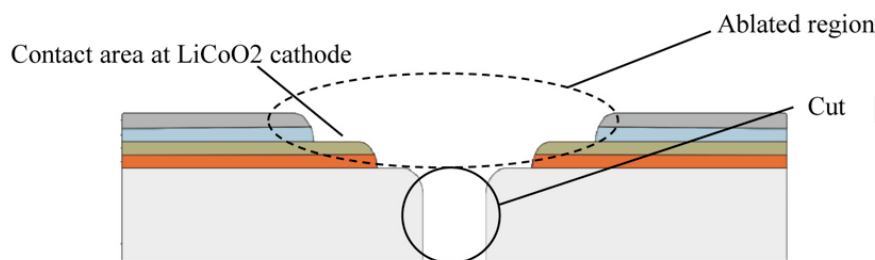


Figure 9. Schematic illustration of conventional cutting and ultrafast laser cutting of SSLB. Reproduced from [20], copyright of SPIE.

In this study, the authors used a nanosecond laser with a wavelength of 1060 nm. The nanosecond laser source has a pulse duration of 27 ns, with a repetition rate of 200 kHz. The diameter of the focused beam is 31 μm, and during laser scanning, a pulse overlap of 84% over the battery's surface was used. For the ultrafast laser ablation of SSLBs in Figure 9, the removal of the LiPON and lithium layers above the LiCoO₂-layer was believed to be caused

by the laser ablation of the underlying LiCoO₂ layer and the different thermal expansions of the LiCoO₂-layer and the LiPON-layer, that results in removing the two top layers by photothermal, photomechanical and blast-off ablation processes. Since the ultraviolet wavelength, 1060 nm, of the laser was used, photochemical ablation will not occur. The results show that it is possible to selectively ablate layers within an SSLB cell to create a clean cutting notch to ensure a shortcut-free decollation. The use of a pulsed laser with a very short pulse duration, such as nano-, pico-, and femtosecond, allows for localized energy deposition, limiting heat spread and preventing significant thermal damage to the surrounding material, leading to cleaner edges with minimal melting or cracking or stress-induced phase changes. Conventional cutting using a continuous laser or knife can induce the melt of different layers or generate residues in the SSLB, causing short circuits, as shown in Figure 9. L. Wach et al. [21] established commercially viable laser-cutting technologies for sulfide-based SSLB components. A picosecond pulsed ytterbium fiber laser with a wavelength of 1030 nm operating at an average power of 50 W was used for their experiments. Compared to a constant wave laser, an ultrashort pulsed laser allows cleaner laser cutting, since it generates a narrow heat-affected zone. The authors studied the influence of pulse frequency, peak power, scanning speed, and laser passes for cutting sulfide-based composite cathodes and solid electrolyte separators. An enhancement in edge quality by the laser, in contrast to mechanical punching, is showed by the authors.

As an advanced machining process, laser cutting for the production of SSLBs has several benefits. (i) Laser cutting can produce high-quality cuts with a narrow heat-affected zone. (ii) Laser cutting can be potentially used in a continuous production line when ultrafast lasers are used. And (iii) laser cutting can be more sustainable and environmentally friendly than mechanical cutting. The primary limitations of laser cutting for SSLBs include thermal damage, because solid-state electrolytes are often sensitive to high temperatures, and laser cutting can generate significant heat, leading to potential degradation of the solid electrolyte material by forming an unwanted phase, impacting battery functionality. For example, sulfide-based solid electrolytes are highly sensitive to moisture and can easily react with air, forming toxic byproducts like hydrogen sulfide. Also, the high heat generated during laser cutting can cause the sulfide solid electrolyte to decompose or undergo phase changes, altering its ionic conductivity and creating defects within the material. To prevent unwanted reactions and released toxic gases, laser cutting of sulfide electrolytes typically utilizes a controlled inert atmosphere in an enclosure. Laser cutting can be scaled-up and adapted to different cell geometries and sizes, enabling flexibility in battery design and production based on specific application needs. The technique can be readily integrated into a high-speed production line after proper laser system configuration and automation. However, many challenges remain, including material compatibility, because different solid electrolyte materials may require specific laser parameters to achieve clean cuts without excessive heat damage, and the need for an inert environment. Careful consideration is needed for factors such as laser types, solid electrolyte material properties, cell geometries, cutting speed, and synchronization with other processing steps to ensure seamless integration within the production line compositions to enable consistent quality and high throughput.

2.5. Other Laser Machining Processes

In SSLBs, the interface resistance between the electrode active materials and solid electrolytes is typically higher than that of liquid electrolytes, which affects the charge (e.g., electrons and ions) transport within SSLBs. High interfacial resistance at the interface also limits their reversible capacity and cycling efficiency. Therefore, it needs to be carefully engineered during the SSBs' fabrication to reduce the interfacial resistance thereafter to

achieve a high-rate performance. S. Yan et al. [22] employed a laser-texturing technique to produce micro-patterns on the side of the $\text{La}_{2/3-x}\text{Li}_{3x}\text{TiO}_3$ solid-state electrolyte that is facing the cathode to increase the surface contact area with the cathode active materials and provide more channels for Li^+ migration at the interface. With the additional help of adding a small amount of liquid electrolyte to fill up the void spaces between the laser-textured $\text{La}_{2/3-x}\text{Li}_{3x}\text{TiO}_3$ and the cathode, the SSLB cell engineering by a laser surface texturing process leads to a decreased interfacial resistance and an improved battery energy density at high C rate. To enable long-term cycling of the SSLBs, the authors believed further optimization of the laser-textured pattern and the establishment of a more stable interface are needed. Watanabe et al. [23] used a picosecond amplified diode-pumped solid-state laser operating at the second-harmonic wavelength of 532 nm to drill holes in the cathode layers and filled the holes with solid-state electrolytes for Li-ion batteries. Due to improvement in the contact between the cathode active material and electrolyte, the cell showed a significant improvement in the rate performance. S Wu et al. [24] used the laser-texturing method to create a repeatedly arranged pore structure on the cathode layer and then induced an in-situ polymerization of the gel electrolyte within the laser-textured cathode. This unique structure enables sufficient interfacial contact between the electrolyte and the cathode active materials and provides improved lithium-ion transport. The cathode that is integrated with the gel electrolyte can effectively reduce the percentage of inactive electrode active materials and help to release the capacity for the thick cathode. The quasi-solid $\text{LiFePO}_4/\text{Li}$ half-cell with active material loading of 8 mg cm^{-2} exhibits good electrochemical performance (i.e., 118.5 mAh g^{-1} after 100 cycles at 0.2 C rate at room temperature). Also, when the quantity of active materials increases to 30 mg cm^{-2} , the $\text{LiFePO}_4/\text{Li}_4\text{Ti}_5\text{O}_{12}$ full cell still has a pretty high discharge capacity (i.e., 105.9 mAh g^{-1} after 400 cycles at 0.2 C rate at room temperature). M. Scheller [25] investigated a laser-ablation process for creating a 3D pore structure on a cathode into which the PEO/LiTFSI solid-polymer electrolyte is filled. They studied the performance of an SSLB cell that incorporates the PEO/LiTFSI solid polymer and LLZO ceramic solid electrolytes with a laser-treated NMC-811 cathode and a Li-metal anode. They found that the SSLBs with laser-structured and electrolyte-filled cathodes have considerable rate capability improvements due to diminished diffusion and interfacial charge transfer resistance. J. Kriegler et al. [26] investigated the use of an ultrashort pulsed laser having different wavelengths, fluences, and pulse repetition rates to create holes, trenches, and cavities on the commercial ceramic solid electrolyte lithium aluminum germanium titanium phosphate. Their results provide insight into the laser ablation behaviors of glass-ceramic materials and contribute the knowledge needed for applying ultrashort pulsed laser ablation in next-generation battery production.

In summary, as a non-contact process, laser material processing offers critical advantages for the sintering, particle generation, surface cleaning, cutting and interfacial engineering of SSLBs' materials and components and provides precision and versatility that are key to advancing battery performance and facilitating the development of next-generation energy storage solutions.

3. Pulsed Laser Deposition Technology for SSLBs

Pulsed laser deposition (PLD) involves using high-energy laser pulses to ablate material from a target, which then deposits as a thin film on a substrate. Excimer lasers and Nd:YAG lasers are commonly used for PLD because of their high pulse energy and industrial track record. The best wavelength for pulsed laser deposition (PLD) depends on the material being deposited. The wavelength of the laser determines how deeply it penetrates the material being deposited. The short wavelength of excimer lasers causes the

light to be absorbed selectively near the surface of the material. This selective absorption leads to fast heating and evaporation, which helps control the stoichiometry and crystal properties of the film. The major advantages of the PLD technique include its controllability, versatility, and consistency, and it can maintain the stoichiometry of the target material during deposition, allowing for a relatively simple deposition of complex materials. PLD is a highly effective technique used in the fabrication of SSLBs, particularly for creating thin films of solid electrolytes, cathodes, and other critical components. The role and benefits of PLD will be illustrated in the following examples.

3.1. PLD of Solid Electrolytes

Garnet-type solid electrolytes, such as $\text{Li}_7\text{La}_3\text{Zr}_2\text{O}_{12}$ (LLZO), show notable stability at high voltage at the cathode side and at the interface with the lithium metal anode. However, there are still challenges relating to the material's stability when it is integrated with other SSLB components under battery operating conditions. To overcome these challenges, a better understanding of the material compatibility and degradation mechanisms of solid electrolytes is needed. Electrochemical characterization of model thin film SSLBs has proven to be a valuable tool for understanding the electrochemical performance of solid electrolytes, as well as the origin of battery degradation or failure caused by interface reactions between the solid electrolyte and the anode or cathode. A whole thin-film SSLB cell can be fabricated by the PLD alone or combined with other thin-film deposition methods. Particularly, those thin-film fabrication methods allow for the deposition of the solid electrolyte layer with appropriate phase, composition, and morphological characteristics and have the advantage of better interfacial contact with the anode and cathode. A variety of thin-film deposition methods, including PLD, radio frequency (RF) sputtering, sol-gel, chemical vapor deposition (CVD), focused ion beam (FIB) milling, atomic layer deposition (ALD), and wet coating, can be used for the preparation of solid electrolyte films [27]. Among those thin-film deposition methods, PLD is the method of choice for the deposition of thin-film solid electrolytes for SSLBs because complex oxide materials constitute the most promising solid electrolytes. M. Saccoccio et al. [28] reported the deposition of crystalline Ta-doped LLZO thin films on MgO (100) substrates via PLD. The Ta-LLZO films of 30 and 50 nm thickness were deposited by the authors using a Nd:YAG laser with the fourth harmonic generation output at a wavelength of 266 nm and repetition rate of 10 Hz, with the fluence at 1 or 4 J cm^2 in the PLD System, as shown in Figure 10a. The short wavelength, 266 nm, of the fourth harmonic Nd:YAG laser allows the light to be absorbed selectively near the surface of Ta-LLZO, leading to better control of the stoichiometry and crystal properties of the films. The authors used electrochemical impedance spectroscopy (EIS) measurements to determine the ionic conductivity of the Ta:LLZO films. For the EIS, two thin (~20 nm) Au strips were deposited on the top of the solid electrolyte film by sputtering, as illustrated in Figure 10b. The ionic conductivity was measured by conducting EIS in a temperature range of 300–500 °C in dry synthetic air. The authors investigated the impact of laser fluence, deposition temperature, and post-deposition annealing on the structural, compositional, and transport properties of the Ta-doped LLZO film and found that a pure cubic LLZO structure appears at the deposition temperature, as low as 50 °C by PLD. Figure 11 exhibits the EIS of an annealed sample that was deposited at 50 °C with a laser fluence of ~1 J cm^2 . Every single spectrum can be interpreted as the sum of two superimposed semicircles tailed by a low-frequency diffusive tail. This matches up with the equivalent circuit model displayed in the top panel of Figure 11, where the two ZARC elements at high and intermediate frequencies are resembled the bulk and the grain boundary resistance, respectively. The low-frequency tail, which is represented by a Warburg element, corresponds to the Li diffusion with blocking electrodes. The sum of

both the bulk and grain boundary resistance was used to calculate the conductivity. The EIS results show the resistance of LLZO films decreases with the measuring temperature. The authors analyzed the EIS results for LLZO films deposited by PLD at different temperatures for both laser fluences of 1 or 4 J cm^2 and found that the deposition temperature does not have a significant impact on the crystal structure and conductivity of LLZO. However, films deposited at the low fluence of 1 J cm^2 had lower conductivity than the films deposited at the high fluence of 4 J cm^2 . The effectiveness of high-temperature post-deposition annealing was also evaluated by the authors. They found that the post-deposition annealing of the LLZO films at 600 °C for 24 h in air improved the film's crystallinity, but annealing caused the appearance of the $\text{La}_2\text{Zr}_2\text{O}_7$ phase due to Li-loss. $\text{La}_2\text{Zr}_2\text{O}_7$ harms the Li-ion conductivity of the films. Therefore, conductivity enhancement after the post-deposition annealing was very limited.

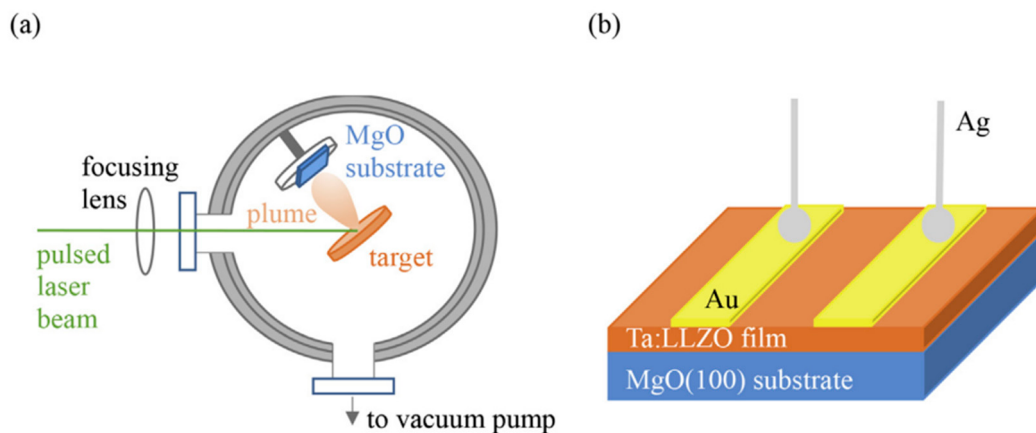


Figure 10. Schematic of the deposition process (a). Experimental set-up for the conductivity measurements (b). Reproduced with permission [28], copyright of Elsevier.

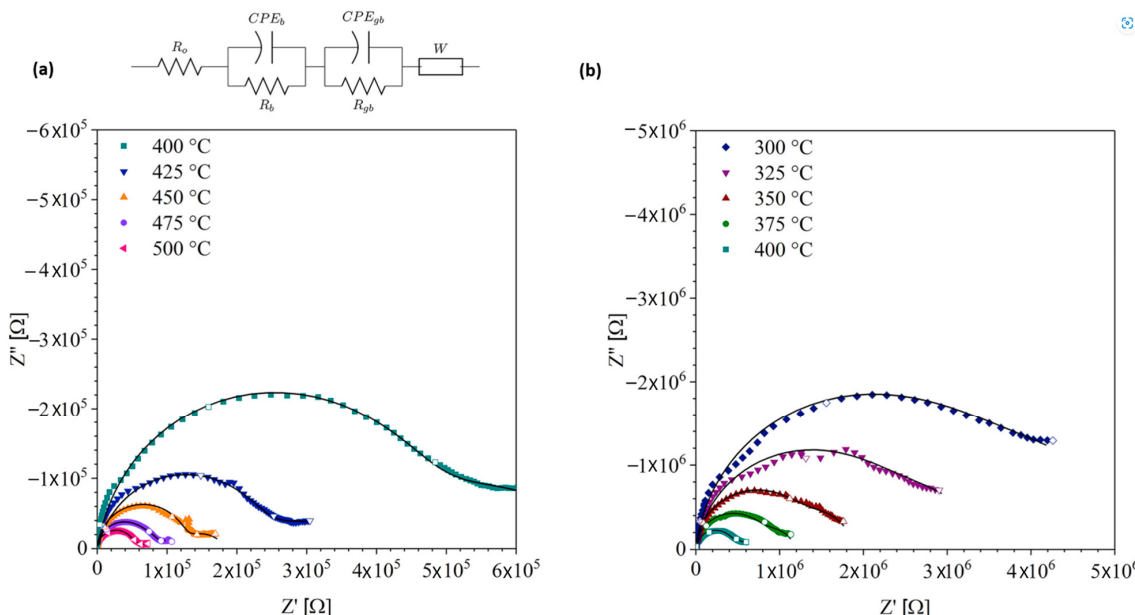


Figure 11. EIS in the ranges 500–400 °C (a) and 400–300 °C (b) for the LLZO films deposited with lower fluence ($\sim 1 \text{ J cm}^2$) at 50 °C and then annealed. The impedance values between 1 and 104 Hz are shown, and the empty markers correspond to the frequencies 1, 10, and 100 Hz. The fits of the data, according to the equivalent circuit model displayed in the top panel, are shown with a black line. Reproduced with permission [28], copyright of Elsevier.

E. Hanc et al. [29] used the PLD technique to fabricate a thin-film $\text{Li}_{6.16}\text{Al}_{0.28}\text{La}_3\text{Zr}_2\text{O}_{12}$ electrolyte by laser ablation of a cubic garnet structure $\text{Li}_{6.16}\text{Al}_{0.28}\text{La}_3\text{Zr}_2\text{O}_{12}$ target with a KrF laser operating at 248 nm, 200 mJ/pulse, and 5 Hz. The short wavelengths of excimer lasers were used to better control the stoichiometry and crystal properties of the $\text{Li}_{6.16}\text{Al}_{0.28}\text{La}_3\text{Zr}_2\text{O}_{12}$ films. The films were deposited on Au-coated fused silica substrates at room temperature in an oxygen pressure of 100–600 mbar. After the deposition, the films were annealed at 700 °C for 15 min to crystallize the film to form garnet structure. Figure 12 shows the impact of oxygen pressure on their X-ray diffraction patterns and phase composition. Films deposited in low oxygen pressure (100 mbar) after annealing at 700 °C gave rise to forming the majority of $\text{La}_2\text{Zr}_2\text{O}_7$ pyrochlore and a low percentage of garnet phase (17 wt%). While increasing the oxygen pressure during PLD, the percentage of the garnet phase increased (maximum garnet content of 66 wt% in 400 mbar of O₂). Further increases in the oxygen pressures (500 and 600 mbar) caused the amorphization of the films, as indicated by the reduced intensity of the diffraction peaks.

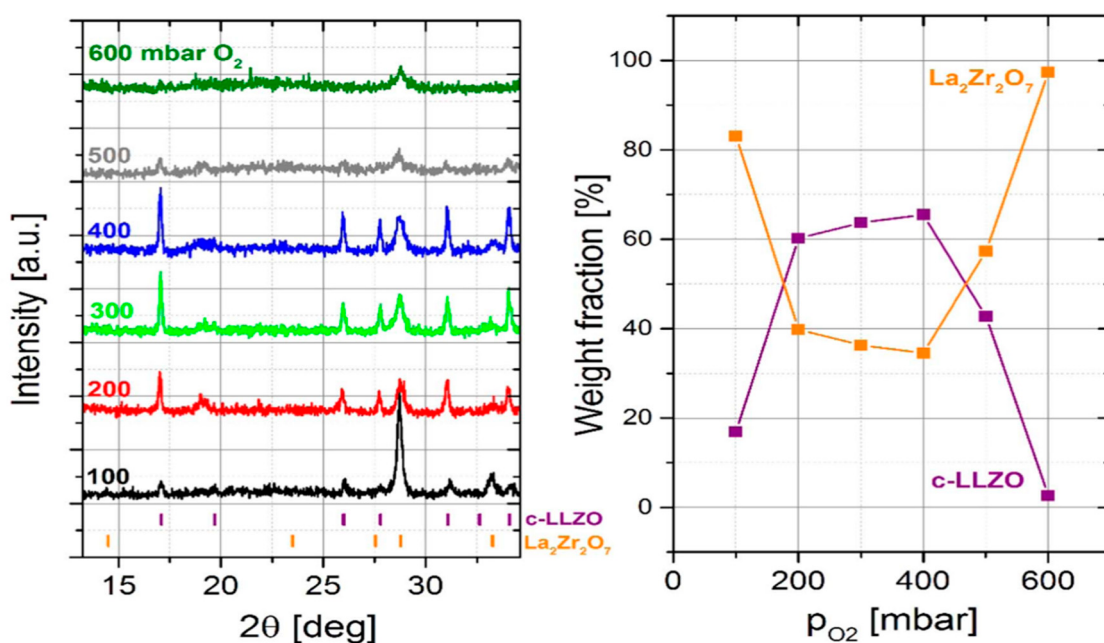


Figure 12. Left pane: X-ray diffraction patterns obtained for LLZO thin films deposited on an Au-coated fused silica substrate at room temperature as a function of oxygen pressure after annealing at 700 °C. Right pane: evolution of the phase composition of the film annealed at 700 °C. Reproduced with permission [29], copyright of Elsevier.

Crystalline lithium lanthanum titanate (LLTO) has a comparably low grain boundary conductivity ($<10^{-5}$ S/cm), which limits its overall material conductivity. In addition, crystalline LLTO is unstable up against lithium metal because lithium insertion will cause a reduction of Ti^{4+} to Ti^{3+} , hence increasing electronic conductivity. Amorphous structural LLTO shows a decrease in the grain-boundary resistance due to its isotropic and non-periodic structure. Amorphous LLTO thin films also have a large voltage stability window, which allows the use of high-voltage cathode materials, such as $\text{LiNi}_{0.5}\text{Mn}_{1.5}\text{O}_4$ spinel. Lee et al. [30] grew amorphous LLTO thin films by PLD using a 248 nm KrF excimer laser with $\sim 2 \text{ J/cm}^2$ energy density and 4 Hz laser frequency on either an interdigitated electrode for conductivity measurement or Pt-coated SiO_2/Si to fabricate an SSLB cell. By controlling the background pressure and temperature, they were able to produce amorphous and low oxygen-deficient LLTO and achieved an optimized ionic conductivity of 3×10^{-4} S/cm and

an electronic conductivity of 5×10^{-11} S/cm. The controllability, versatility, consistency, and stoichiometry conservation of the PLD technique have been demonstrated in this study.

Among the various kinds of solid electrolytes, sulfide-based solid electrolytes are also favorable because of their high Li⁺ conductivities at room temperature. Li₂S-P₂S₅ sulfide glasses prepared by the melt-quenching method are identified as lithium-ion conductors which have high conductivities over 10^{-4} S cm⁻¹ at room temperature [31]. Electrode active material particles coated with the sulfide electrolyte to form a composite electrode for SSLBs are considered to be an effective way to improve the performance of SSLBs due to the formation of an ideal electrode active material-electrolyte interface. The ionic conductivity can be further improved by heat treatment of the sulfide electrolyte-coated active material particles to decrease the voids in the composite electrode. The decrease in the voids can effectively increase the Li⁺ conduction paths. Aso et al. [31] used PLD with a KrF excimer laser to coat the Li₂S-P₂S₅ solid electrolyte onto a NiS-VGCF (VGCF—vapor-grown carbon fiber) composite. A pelletized mixture of Li₂S and P₂S₅ powder with a molar ratio of 80:20 was used as a target by the authors for the PLD. The PLD technique allows the deposition of a stoichiometry Li₂S-P₂S₅ thin film onto NiS-VGCF so that its high Li⁺ conductivity can be maintained. The authors fabricated laboratory-scale SSLB cells by mixing Li₂S-P₂S₅-coated NiS-VGCF with Li₂S-P₂S₅ solid electrolyte as the cathode. For comparison, a cathode that consisted of mixing the uncoated NiS-VGCF with Li₂S-P₂S₅ electrolyte was also fabricated and used in the SSLBs. Figure 13 shows the schematic diagram of the composite cathode. The carbon fiber constructs a continuous electron-conducting path in the composite electrode, while active materials with a uniform size connect intimately with both carbon fiber and solid electrolyte to form an integrated cathode, as shown in the figure.

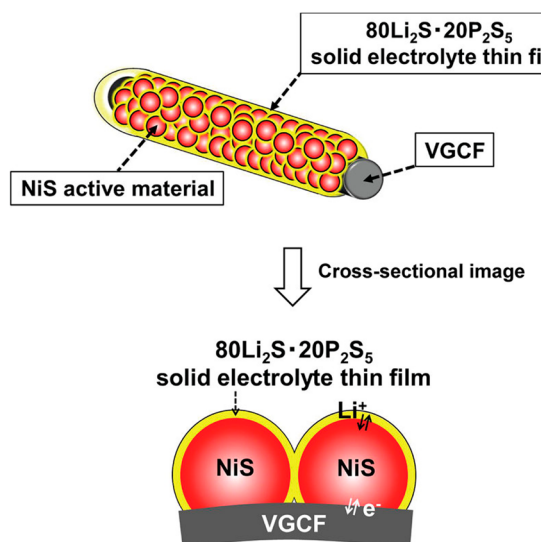


Figure 13. Schematic illustration of the Li₂S-P₂S₅-coated NiS-VGCF composite. Li₂S-P₂S₅ denotes to the 80Li₂S-20P₂S₅ (mol %) solid electrolyte. Reproduced with permission [31], copyright of American Chemical Society.

Two-electrode cells were assembled by the authors using this prepared cathode, a glass solid electrolyte, and a Li-In alloy anode. The three layers were sandwiched by two stainless-steel disk current collectors to form an SSLB cell. Electrochemical tests were conducted using charge–discharge measurements under a constant current density of 3.8 mA cm⁻² at 25 °C in an Ar atmosphere. Panels a and b in Figure 14 display the charge–discharge curves of the SSLB cell using the uncoated or Li₂S-P₂S₅-coated NiS-VGCF composite cathode at the 1st, 2nd, and 50th cycles with the current density of 3.8 mA cm⁻²

(corresponding to ca. 1 C rate). The discharge capacity of the cell with the $\text{Li}_2\text{S-P}_2\text{S}_5$ -coated NiS-VGCF composite is larger than that of the cell with the uncoated NiS-VGCF composite at all cycles. Figure 14c shows the cyclic performance of the SSLB cells at the current density of 3.8 mA cm^{-2} . The SSLB cell fabricated using the $\text{Li}_2\text{S-P}_2\text{S}_5$ -coated NiS-VGCF composite as a cathode showed an initial discharge capacity of 300 mAh g^{-1} and showed clearly better cycle performance than the cell using the uncoated NiS-VGCF composite ($\sim 100 \text{ mAh g}^{-1}$). The authors suggest that the construction of close-contact interfaces among NiS, VGCF, and $\text{Li}_2\text{S-P}_2\text{S}_5$ gives favorable electronic and Li^+ conduction paths in the SSLB cell (see Figure 13). The formation of Li^+ conduction paths was not sufficient in the cathode with 100 wt% $\text{Li}_2\text{S-P}_2\text{S}_5$ -coated NiS-VGCF composites but without adding $\text{Li}_2\text{S-P}_2\text{S}_5$. The addition of $\text{Li}_2\text{S-P}_2\text{S}_5$ particles in the cathode was essential to achieve high performance of the SSLBs.

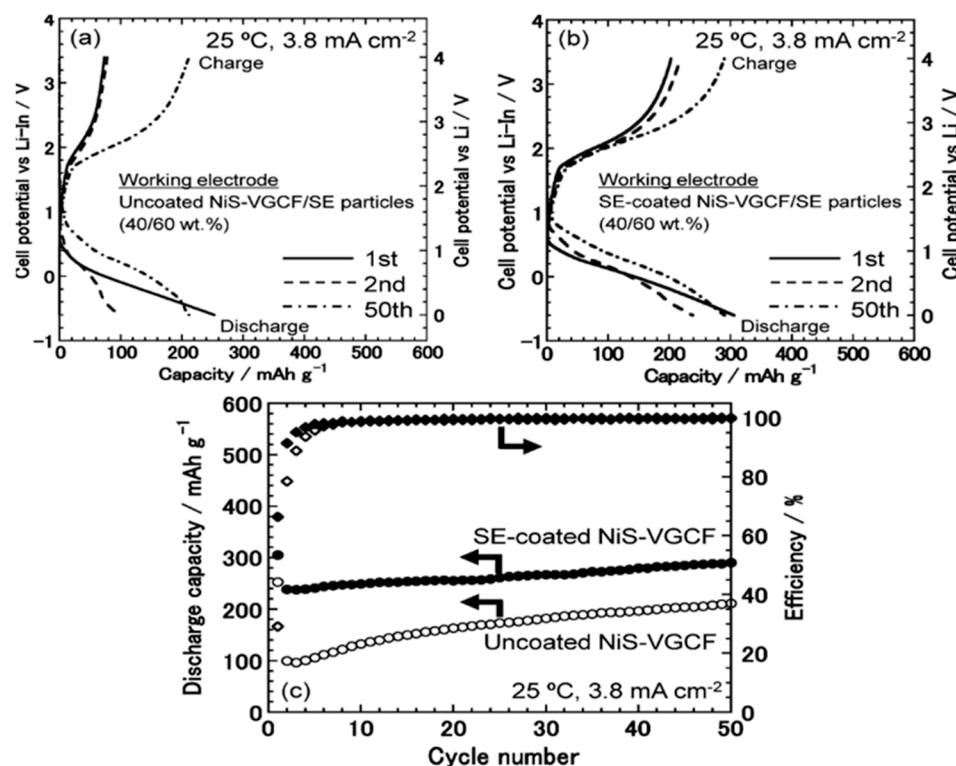


Figure 14. Charge–discharge curves of an SSLB cell using (a) uncoated or (b) $\text{Li}_2\text{S-P}_2\text{S}_5$ -coated NiS-VGCF composite at the 1st, 2nd, and 50th cycles under the current density of 3.8 mA cm^{-2} . (c) Cycle performance of SSLBs using the uncoated or $\text{Li}_2\text{S-P}_2\text{S}_5$ -coated NiS-VGCF composite at the current density of 3.8 mA cm^{-2} (corresponding to ca. 1 C rate). Reproduced with permission [31], copyright of American Chemical Society.

The $\text{Li}_2\text{S-P}_2\text{S}_5$ solid electrolyte was also coated onto LiCoO_2 active material particles by the PLD using a KrF excimer laser by A. Sakuda et al. [32]. In their study, LiCoO_2 particles were pre-coated with a LiNbO_3 film, followed by the coating of $\text{Li}_2\text{S-P}_2\text{S}_5$. Heat treatment of the $\text{Li}_2\text{S-P}_2\text{S}_5$ -coated LiCoO_2 was performed in an Ar atmosphere. An SSLB cell with the structure In/80Li₂S·20P₂S₅/LiCoO₂ was constructed to investigate the electrochemical performance of 80Li₂S·20P₂S₅ solid electrolyte-coated LiCoO_2 . Figure 15 shows charge–discharge curves at a current density of 0.13 mA cm^{-2} of the SSLB using composite electrodes composed of 90 wt.% uncoated, LiNbO_3 -coated, or $\text{Li}_2\text{S-P}_2\text{S}_5$ -coated LiCoO_2 , respectively, with 10 wt.% $\text{Li}_2\text{S-P}_2\text{S}_5$ particles. Their capacities were 20, 60, and 95 mAh g^{-1} , respectively. The capacities of the SSLBs were highest for the cell using 10 wt.% $\text{Li}_2\text{S-P}_2\text{S}_5$ particles and the $\text{Li}_2\text{S-P}_2\text{S}_5$ -coated LiCoO_2 . The authors believed that, in the composite

electrode, the $\text{Li}_2\text{S}-\text{P}_2\text{S}_5$ coated LiCoO_2 particles formed an effective electrode–electrolyte interface and the lithium-ion conducting path to the LiCoO_2 particles. Y. Ito et al. [33] also reported the deposition of amorphous $\text{Li}_2\text{S}-\text{P}_2\text{S}_5$ and $\text{Li}_2\text{S}-\text{GeS}_2$ thin films on LiCoO_2 particles by PLD. In their study, SSLBs using LiCoO_2 particles coated with $\text{Li}_2\text{S}-\text{GeS}_2-\text{P}_2\text{S}_5$ thin films were constructed for charge–discharge performance tests, and the results also show that the SSLBs using heat-treated $\text{Li}_2\text{S}-\text{GeS}_2-\text{P}_2\text{S}_5$ -coated LiCoO_2 particles were found to have a larger capacity than that using uncoated LiCoO_2 particles.

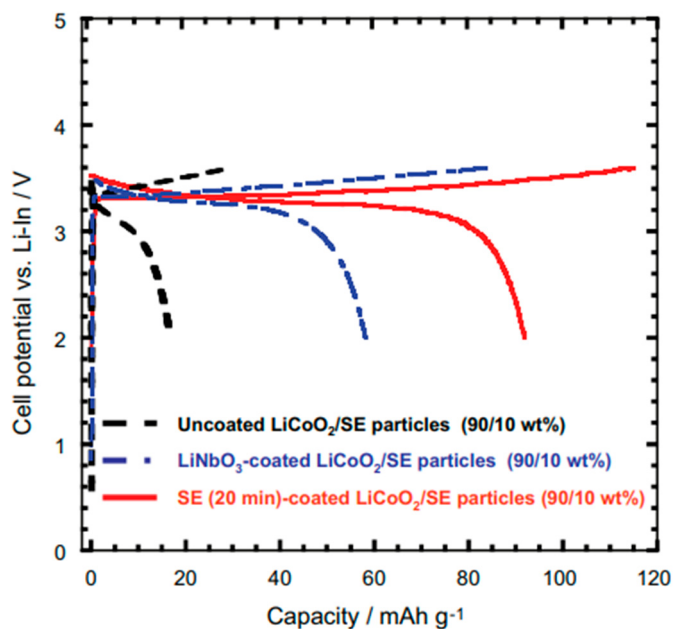


Figure 15. Charge–discharge curves of all-solid-state cells based on composite electrodes with 90 wt.% LiCoO_2 and 10 wt.% solid electrolyte particles. Reproduced with permission [32], copyright of Elsevier.

The ionic conductivity of the amorphous $50\text{Li}_4\text{SiO}_4\cdot50\text{Li}_3\text{PO}_4$ (mol%) solid electrolyte film was $1.6 \times 10^{-6} \text{ S cm}^{-1}$ at room temperature, which is higher than the conductivity of Li_3PO_4 and Li_4SiO_4 films. Y. Sakurai et al. [34] used PLD with a KrF excimer laser to coat a $50\text{Li}_4\text{SiO}_4\cdot50\text{Li}_3\text{PO}_4$ film onto LiCoO_2 active material particles. They built an SSLB cell with the structure of $\text{Li-In}/80\text{Li}_2\text{S}\cdot20\text{P}_2\text{S}_5/\text{LiCoO}_2$ (uncoated and $50\text{Li}_4\text{SiO}_4\cdot50\text{Li}_3\text{PO}_4$ coated). The electrochemical performance of the SSLB cells was then investigated with electrochemical impedance spectroscopy and charge–discharge cycling. Figure 16a shows the impedance spectra of the SSLB cells with uncoated and $50\text{Li}_4\text{SiO}_4\cdot50\text{Li}_3\text{PO}_4$ -coated LiCoO_2 after going through the first charge process at 0.13 mA cm^{-2} with the cut-off voltage of 3.6 V (vs. Li-In). The cells show three resistance components in the high, middle, and low-frequency regions. The resistances in the high-frequency region ($>10 \text{ kHz}$), middle-frequency region (the peak top frequency of 1 kHz), and low-frequency region (the peak top frequency of 1 Hz) are ascribed to the resistance of the $\text{Li}_2\text{S}-\text{P}_2\text{S}_5$ electrolyte layer (RSE), the interface between LiCoO_2 and the electrolyte (RPE), and the Li-In (RNE), respectively. Two components of RSE at $>10 \text{ kHz}$ and RNE at 1 Hz are almost the same in the two cells. The RPEs of uncoated and $50\text{Li}_4\text{SiO}_4\cdot50\text{Li}_3\text{PO}_4$ -coated LiCoO_2 are 190 and 48Ω , respectively, indicating that by coating $50\text{Li}_4\text{SiO}_4\cdot50\text{Li}_3\text{PO}_4$ on the LiCoO_2 active materials the RPE was decreased significantly. The authors believed that the high Li^+ conductivity of $50\text{Li}_4\text{SiO}_4\cdot50\text{Li}_3\text{PO}_4$ thin accounts for the significant decrease in the interfacial resistance of the SSLBs. Discharge measurement of the SSLB cells at the high current density of 6.4 mA cm^{-2} was also carried out after charging the cells to 4.2 (vs. Li-In). Figure 16b shows that the discharge capacity, 46 mAhg^{-1} , of the SSLB cell with

$50\text{Li}_4\text{SiO}_4 \cdot 50\text{Li}_3\text{PO}_4$ -coated LiCoO_2 is higher than that of the cell with uncoated LiCoO_2 , 33 mAh g^{-1} . The decrease of the interfacial resistance by $50\text{Li}_4\text{SiO}_4 \cdot 50\text{Li}_3\text{PO}_4$ coatings with high Li^+ conductivity reduces the IR drop, resulting in a high voltage plateau, which leads to a large capacity at the discharge process. From the research works mentioned above, it is obvious that a coating of electrode active material particles with a highly conductive solid electrolyte by PLD is an effective way to decrease the electrode–electrolyte interfacial resistance, which is a promising way to create power density and high-performance SSLBs.

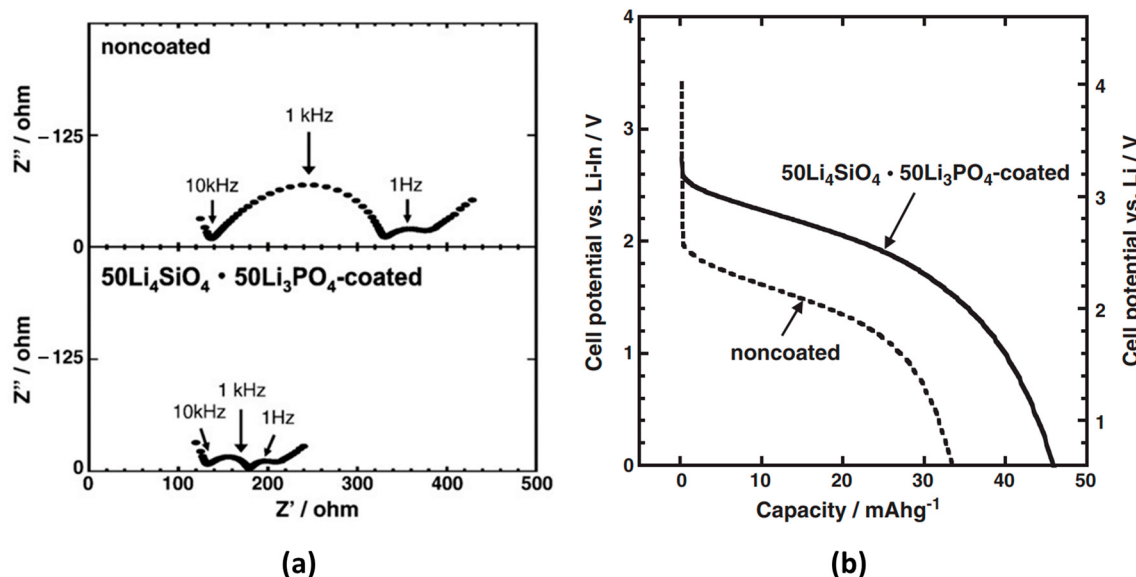


Figure 16. (a) Impedance profiles of the all-solid-state cells with noncoated and $50\text{Li}_4\text{SiO}_4 \cdot 50\text{Li}_3\text{PO}_4$ -coated LiCoO_2 after the first charge process. The cells were charged at 0.13 mA cm^{-2} , and the cut-off voltage was 4.2 V (vs. Li). (b) Discharge curves of all-solid-state cells with noncoated and $50\text{Li}_4\text{SiO}_4 \cdot 50\text{Li}_3\text{PO}_4$ -coated LiCoO_2 . The cells were discharged at 6.4 mA cm^{-2} and the cutoff voltage was 0 V . Adopted with permission from [34], copyright of Elsevier.

While PLD offers significant advantages for the fabrication of solid electrolytes based on metal oxides and sulfides, the potential of using PLD to fabricate halide-based materials, such as Li_3MCl_6 ($\text{M} = \text{In}, \text{Er}, \text{Sc}, \text{Ho}, \text{Y}$) for SSLBs remains largely untapped. Considering that PLD has been used to fabricate halide photovoltaic cells, particularly those based on perovskite materials, it is anticipated that the technique will also offer significant advantages for the exploitation of halide-based materials. However, not all materials are suitable for PLD. Some halide materials may decompose or undergo unwanted phase changes when subjected to the high-energy laser ablation process, potentially affecting the quality and performance of the deposited films. Halide and lithium are both highly volatile, which can also lead to challenges in maintaining stoichiometry during deposition. This requires careful optimization of deposition parameters such as laser energy and substrate temperature as well as target compositions. In summary, PLD allows for the deposition of high-quality, dense, and uniform thin films or coatings, which are crucial for the performance of solid electrolytes in SSLBs. These films can achieve the necessary ionic conductivity and mechanical stability. The PLD technique is also compatible with a wide range of materials, including complex oxides and sulfides, which are used as the solid electrolytes for SSLBs, as demonstrated in the examples mentioned above. This versatility facilitates the exploration of novel materials with enhanced properties. PLD provides precise control over the stoichiometry of the deposited films and coatings, ensuring that the chemical composition closely matches that of the target material. This control is essential for optimizing the ionic conductivity and stability of the solid electrolyte. The

process parameters, such as laser energy, substrate temperature, and ambient gas pressure, can be finely tuned to influence the microstructure and properties of the PLD-deposited films or coatings. This flexibility allows researchers to tailor the electrolyte characteristics to specific battery requirements. For the deposition of solid electrolyte thin films, PLD stands out for its ability to deposit complex materials with better control over composition and microstructure, while methods like chemical vapor deposition (CVD) and atomic layer deposition (ALD) provide conformal coatings with excellent film uniformity. PLD has a relatively low deposition rate and could be more costly to scale-up for large-scale applications. CVD can achieve a very high deposition rate and is easier to scale-up for large-scale applications. However, it typically requires higher temperatures than PLD and can be challenging to control the purity of the deposited film. ALD has the advantage of precise thickness control but has a relatively slow deposition rate compared to PLD and CVD. The technique can be more costly and complex to set up and optimize than PLD and CVD techniques. Sputtering can produce solid electrolyte films with excellent uniformity and good adhesion to the anode or cathode, similar to PLD. However, the technique can sometimes lead to compositional changes in the deposited film, especially for complex solid electrolyte materials, such as mixed metal oxides or sulfides. Electroplating could be used to deposit a layer of solid electrolytes onto a conductive substrate such as Li metal through an electrochemical process. It offers cost-effectiveness, but the technique sacrifices quality and uniformity for the low cost.

3.2. PLD of Active Materials for Cathode

The main advantage of using PLD to fabricate a cathode for SSLBs is its ability to precisely control the chemical composition and morphology of complex sulfide or oxide cathode materials with tight stoichiometry requirements, which is crucial for high performance in SSLBs. The high energy of the laser pulse can also generate nanoparticles during ablation, leading to the deposition of fine-grained cathode materials with large surface areas, enhancing the Li^+ diffusion kinetics. By carefully adjusting the deposition parameters, PLD allows for the precise control of the interface between the cathode and the solid electrolyte, minimizing interfacial resistance and improving electrochemical performance. It can also be used to deposit complex cathodes with multilayer structures such as a cathode layer with additional protective layers or with graded compositions. Compared to other deposition techniques, PLD often requires lower processing temperatures, which can be beneficial for temperature-sensitive materials and substrates. T. Matsuyama et al. [35] deposited an amorphous TiS_4 (a- TiS_4) thin film by PLD using a KrF excimer laser operating at 2 J/cm^2 on target energy density and a 5 Hz pulse repetition rate on the garnet-type $\text{Li}_7\text{La}_3\text{Zr}_2\text{O}_{12}$ (LLZO) solid electrolyte pellet. The authors first prepared the LLZO electrolyte by a sol-gel process, followed by calcinating, ball-milling, pressing, and sintering. The lithium-ion conductivity of the prepared LLZO pellet was determined to be $2\text{--}4 \times 10^{-4} \text{ S cm}^{-1}$ at room temperature. Figure 17a shows the cross-sectional SEM image of the interface between an a- TiS_4 thin film electrode and an LLZO electrolyte pellet. The ~400 nm TiS_4 thin film deposited by PLD was dense and attached firmly to the LLZO pellet, giving good contact between the electrode and the electrolyte. After producing the a- TiS_4 thin-film electrodes, the Au current collector was deposited on the top of the a- TiS_4 thin-film electrodes by the vacuum vapor deposition. Subsequently, the Li thin-film electrodes were deposited onto the other surface of the LLZO pellets by the same method. Finally, the Li foil, as the negative electrode, was pushed tightly on the Li thin-film electrode. The prepared pellets were sandwiched with two stainless-steel rods to form an SSLB cell, Li/cubic-LLZO/a- TiS_4 , and the SSLB cell was evaluated by charging–discharging cycles at 25 °C.

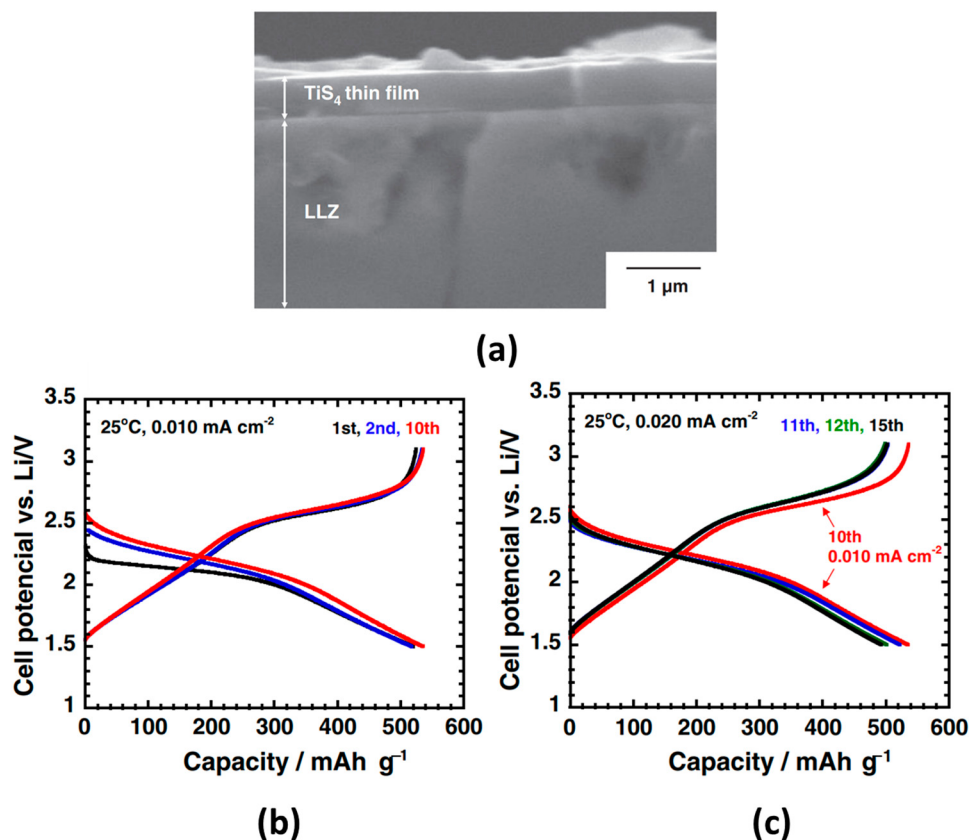


Figure 17. Cross-sectional SEM image of a-TiS₄ thin-film electrodes on LLZO pellet (a), and charge–discharge curves of the all-solid-state cell Li/cubic-LLZO/a-TiS₄ at the current density of 0.010 mA cm⁻² for initial 10 cycles (b) and at 0.020 mA cm⁻² after the 11th cycle (c). Adopted with permission from [35], copyright of Elsevier.

The charge–discharge curves of the SSLB cell are exhibited in Figure 17b,c. Charge–discharge measurements of the cell were conducted at the current density of 0.010 mA cm⁻² from the 1st cycle to the 10th cycle, and the cell potential vs. capacity curves are shown in Figure 17b. The current density was then increased to 0.020 mA cm⁻² from the 11th cycle to the 15th cycle, and the results are shown in Figure 17c. The 10th charge–discharge curves are presented in Figure 17c for comparison as well. The charge capacity was about 500 mAh·g⁻¹ at the first cycle, and the capacity fading was not observed at 0.010 mA cm⁻² for the first 10 cycles. The reversible capacity was declined by about 40 mAh·g⁻¹, when the current density increased from 0.010 mA cm⁻² to 0.020 mA cm⁻². Interfacial resistance between the a-TiS₄ electrode and the LLZO electrolyte was nearly constant during charge–discharge cycling. The results show that the PLD method can deposit a high-performance amorphous TiS₄ thin-film cathode electrode without a heat-treatment process, which is attractive for the fabrication of SSLBs with the LLZO electrolyte.

Various metal oxides, such as LiCoO₂, Li(Ni,Co)O₂, LiMn_xNi_{2x}O₄, and LiFePO₄, have been exploited as cathode active materials for SSLBs. Among these materials, LiCoO₂ (LCO) with a layered rocksalt structure exhibits a highly reversible Li⁺ intercalation reaction. S. Shiraki et al. [36] used single-crystal Au (110) and Pt (110) as the substrates for the deposition of epitaxial LCO thin films by PLD. The Au and Pt (110) surfaces were selected as the substrates since the reconstructed (110) surfaces consist of alternately arrayed {111} nanofacets, which lowers the total surface energy to facilitate the growth of the epitaxial LCO films, which show a difference in the charge–discharge capacity depending on their crystal orientation. The authors established a process to control the LCO crystal orientation that is beneficial for smooth Li⁺ insertion/extraction reactions. In their PLD experiments,

a KrF excimer laser with a repetition rate of 5 Hz and a fluence of 1.0 J cm^{-2} was used as the energy source, and a polycrystalline $\text{Li}_{1.2}\text{CoO}_2$ was used as the target. During the deposition, the oxygen partial pressure was kept at 1×10^{-6} Torr, and the substrate temperature was kept at room temperature. The as-grown films are $\sim 200 \text{ nm}$ thick and were subsequently annealed at 650°C in the air to obtain a high-temperature LCO phase. The XRD and TEM results confirm the epitaxial growth of LCO thin films having three different types of crystal orientations, in which the c-axes of the LCO are tilted to the surface normal.

The authors then fabricated an SSLB cell by subsequently depositing a thin-film LiPON solid electrolyte by RF magnetron sputtering (RFMS) and a thin-film Li anode by vacuum thermal evaporation (VTE) on the top of the LCO/Au(110). A schematic illustration of the all-solid-state thin-film batteries is shown in Figure 18a. Subsequent to the deposition of LiPON onto the LCO, the films were annealed at 180°C for 30 min in Ar to reduce the interface resistance between the LiPON and the LCO. The CV curves of the Li/LiPON/LCO/Au(110) SSLB cell in Figure 18b show several sharp current peaks (C1–4, D1–3), whose peak voltage locations do not change with the scan number, indicating good stability and repeatability in the charging–discharging operation. In Figure 18c, the CV curves of the Li/LiPON/LCO/Pt(110) show the same features as Figure 18b, with the CV peak voltage locations and peak separations being almost the same as that found for the Li/LiPON/LCO/Au(110) cell. The CV curves of Figure 18b,c show sharp CV peaks with small peak separations in the forward and revised cycling, which resulted from the well-defined epitaxial single-crystal structure of the LCO thin films. For the LCO with polycrystalline structures, much broader CV peaks and a larger peak separation were found by the authors. Those results show that the epitaxial thin films deposited by PLD offer ideal well-defined interfaces between the solid-state electrolyte and the electrode active materials for studying the electrochemical charging–discharging reactions and Li transport mechanisms in the SSLBs.

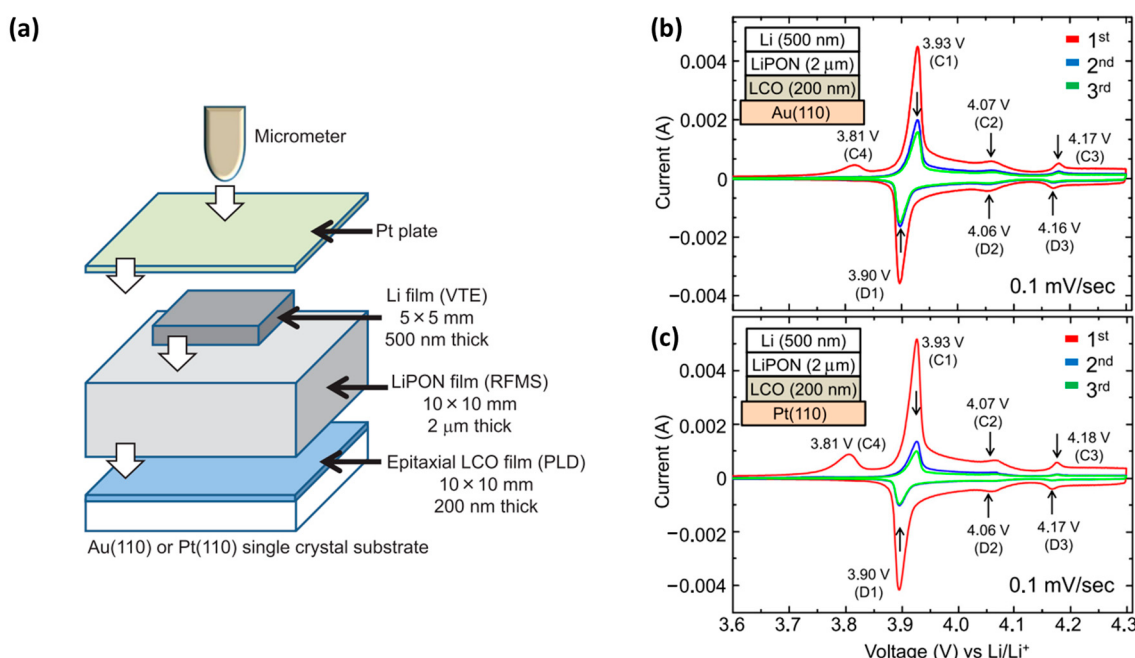


Figure 18. Schematic image of all-solid-state thin-film batteries using epitaxial LiCoO_2 thin films on single crystal (110) substrates of Au and Pt (a) and cyclic voltammogram of thin-film solid-state battery of Li/LiPON/epitaxial LiCoO_2 on Au(110) (b) and on Pt(110) (c). The insets show the multilayered thin-film SSLBs. Adopted with permission from [36], copyright of Elsevier.

Although LCO is the most studied cathode material, other lithium-rich layered materials, such as Li_2RuO_3 , which has a similar crystal structure as that of LCO, were also recognized as promising cathode materials for SSLBs. The lithium ions in the RuO_6 layers can also participate in the intercalation reaction, leading to a potentially high theoretical capacity. Y. Zheng et al. [37] grew epitaxial $\text{Li}_2\text{RuO}_3(001)$ thin films on $\text{Al}_2\text{O}_3(0001)$ substrates by PLD using a 248 nm KrF excimer laser. A Li_3PO_4 solid electrolyte layer was then deposited on the epitaxial Li_2RuO_3 cathode film by RF magnetron sputtering, followed by vacuum evaporation deposition of the In or Li anode film to form an SSLB cell. Figure 19a presents a schematic illustration of the assembled SSLB cell. The STEM image (Figure 19b) of the In/ Li_3PO_4 / Li_2RuO_3 cell confirms that these three layers are all dense and flat. The electrochemical properties of the assembled cell are evaluated by CV and charge–discharge measurements. Two anodic peaks at 2.9 and 3.2 V and two cathodic peaks at 2.6 and 2.9 V are found in the CV curves, which are attributed by the authors to lithium (de)intercalation out of or into the Li_2RuO_3 film (Figure 19c). The solid-state battery exhibits charge and discharge capacities of 101.7 and 85.8 mAh g^{-1} at the 4th cycle, respectively (Figure 19d), and gradual capacity fading is observed up to the 13th cycle. The authors also used Li metal to replace In as the anode and investigated the charge–discharge characteristics of the battery. Figure 19e presents changes in the discharge capacity of the Li/ Li_3PO_4 / Li_2RuO_3 cell vs. the cycle number and the C-rate. The capacity of the cell was examined at 0.1 C (1.67 mA cm^{-2}) for the initial 30 cycles, and then, the current densities increased from 0.1 C to 0.5 C, 1 C, 2 C, 5 C, 10 C, and 20 C. At each C rate, the capacity was recorded for every five cycles. Although the discharge capacity significantly decreases as the C rate increases, the discharge capacity at 20 C is still high, i.e., 63% of the capacity at 0.1 C rate. This result reveals that very homogeneous anode–solid electrolyte and solid electrolyte–cathode interfaces were formed by thin-film deposition techniques, such as PLD, sputtering, and vapor evaporation on the SSLB cell. The excellent interfaces facilitate lithium intercalation and deintercalation processes. The authors also found that the cycle performance and the rate capability of the novel Li_2RuO_3 cathode are comparable to that of the LiCoO_2 cathode in SSLBs. The results demonstrated that those lithium-rich layered rock salt oxides could also be excellent candidate materials for the cathode in high-capacity SSLBs.

In summary, PLD is capable of depositing high-quality thin films of a wide range of materials, including metal oxides and sulfides. This versatility allows for the exploration and use of advanced materials, such as multi-element metal oxides/sulfides or doped metal oxides/sulfides, that can enhance the performance of SSLBs’ cathode active materials. The technique also offers stoichiometry conservation of the deposited films, vital for optimizing the electrochemical properties of cathode active materials. PLD provides precise control over the film’s thickness and composition, which is crucial for the rapid prototyping and testing of new materials and structures, accelerating research and development efforts in SSLBs. Although PLD is a critical technique in the development of SSLBs, some challenges associated with PLD for cathode fabrication do exist, including (i) scaling up PLD for large-scale SSLB production can be challenging due to the limited deposition surface area achievable with a single laser beam; (ii) maintaining uniform deposition over a large substrate area is difficult and requires careful optimization of laser parameters and target design, which limits its industrial fabrication for SSLBs; and (iii) PLD systems can be complex and expensive compared to other SSLB fabrication techniques.

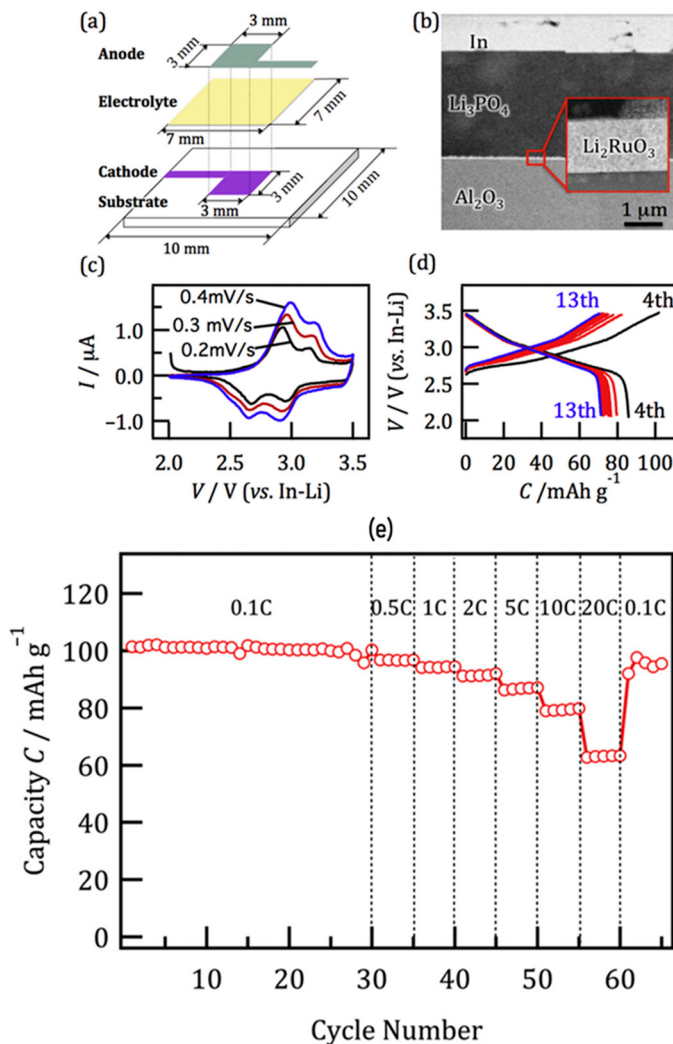


Figure 19. (a) Schematic of the cell design, (b) STEM image of the device cross-section, (c) CV plots at scan rates of 0.2–0.4 mV s^{-1} , (d) charge–discharge plots collected at 1.1 mA cm^{-2} for an In/ Li_3PO_4 / Li_2RuO_3 all-solid-state battery, and (e) variations in discharge capacity retention of a Li/ Li_3PO_4 / Li_2RuO_3 all-solid-state battery with cycle number and charge–discharge C rates. The voltage range was 3.0–4.0 V. Adopted with permission from [37], copyright of Elsevier.

4. Conclusions and Future Perspectives

SSLBs have the potential to offer significantly higher energy density compared to traditional lithium-ion batteries and eliminate the safety concerns related to flammable liquid electrolytes. Laser material processing is considered a promising manufacturing technology for advancing the overall cell performance and stability of SSLBs because it allows for enhanced material properties such as density and surface morphology, improving ionic conductivity and reducing interfacial resistance within the battery materials, layers, and components. Several key conclusions and future perspectives emerge from this mini-review

4.1. Conclusions

Laser material processing is adaptable to a wide range of materials, including metal oxides, metal sulfides, polymers, and metals, making them suitable for processing various components in SSLBs, such as electrodes, electrolytes, and current collectors. Laser beams offer unparalleled simplicity and precision in the processing of materials, allowing for the precise cutting, patterning, drilling, surface cleaning, and surface modification of SSLBs' components, which are crucial for advancing this energy storage technology. Laser

material processing can also improve the physical and chemical properties of materials used in SSLBs, such as (i) to clean and densify ceramic solid electrolytes, enhance interfacial adhesion to reduce interfacial electrical resistance; (ii) to modify surface morphology and crystal structure to improve ion conductivity; (iii) to engineer the interface between the solid electrolyte and the anode or the cathode to optimize the Li⁺ conductivity and diffusion pathways; (iv) to produce high-quality cuts with a narrow heat-affected zone, which is needed in a SSLB continuous production line; and (iv) to deposit high-quality thin films of a wide range of cathode materials, which allows for the exploration and use of advanced materials to enhance the performance of SSLBs. While laser material processing can potentially improve many aspects of SSLBs, there are several limitations, including (i) precisely controlling the laser beam to modify only the desired interface without causing damage to the surrounding materials can be difficult; (ii) localized heating from the laser can create thermal stress within the battery components, leading to cracks or delamination, especially in SSLBs' multi-layered structures; (iii) laser penetration depth can be limited, making it challenging to modify thicker solid-state electrolyte layers uniformly; and (iv) implementing laser material processing on a large scale for the mass production of SSLBs can be costly and complex.

4.2. Future Perspectives

Developing cost-effective and scalable manufacturing processes for SSLBs is crucial for their widespread adoption. Laser material processing could be integrated with the R2R battery manufacturing processes, such as printing (e.g., screen printing, inkjet printing, and 3D printing), wet-coating (e.g., tape casting and slot-die coating), pressing (e.g., cold/low temperature pressing and high temperature and cold sintering) and thin-film vapor deposition processes (e.g., PLD, ALD, sputtering, thermal evaporation, and other vacuum deposition processes) offering the potential for automation, precision, and high throughput, which can contribute to efficiency, cost reduction, and scalability. For example, ultra-short lasers like pico- to femtosecond lasers enable selective material removal with minimal heat generation, allowing precise cutting or patterning of anode, cathode, and solid electrolyte layers of various materials in SSLBs to facilitate the creation of a single cell in a roll. Laser annealing/sintering processes could be integrated into the R2R production line to adjust the crystalline phases of electrode and electrolyte materials, optimize their properties, and improve their interface during the printing or coating processes to improve their electrochemical performance. Laser surface cleaning could also be used to clean the surface of the solid electrolyte layer in the R2R production line before printing or depositing the anode or cathode layer. The technique can be used to prepare welding areas by removing surface contaminants to strengthen welds and improve their overall quality. By combining with other thin-film deposition methods and laser processing techniques, PLD could be used to produce thin-film SSLB packs, where the electrodes, solid electrolytes, and electrical contact (i.e., current collectors) could be deposited and machined on flexible substrates continuously in an R2R manufacturing line in a vacuum chamber to ensure a clean environment, leading to higher quality thin-film SSLBs. The non-contact nature of laser processing reduces the risk of contamination and damage to the underlying substrate. Combining laser material processing with other technologies, such as 3D printing, can lead to even more innovative and efficient battery designs. Laser processing is a high-throughput process that is suitable for integration with the large-scale R2R manufacturing line, which could also lead to more automated and flexible manufacturing lines and offer cost-effectiveness and efficient material utilization, which is particularly important to make SSLBs commercially viable.

Further research into new solid electrolyte materials with high ionic conductivity and good compatibility with electrodes is crucial for the future development of SSLBs. Laser material processing could facilitate the development and testing of novel materials for SSLBs. For example, PLD can be used to rapidly prototype and evaluate new electrolyte and electrode materials in the model thin-film SSLBs since the technique can fabricate high-quality electrodes and electrolyte layers and their interfaces. Laser material-processing techniques such as texturing, ablation, and patterning could also be employed to create optimized electrode and electrolyte structures with an enhanced surface area and porosity. Optimizing the interface between the electrodes and the solid electrolyte is essential for achieving high performance and safety for SSLBs. Laser material-processing techniques such as drilling, surface cleaning, and ablation could be used to control the morphology and composition at the electrode–electrolyte interface, which helps suppress the formation of lithium dendrites, a major safety concern in SSBs. Continued research into faster and more powerful new lasers will likely lead to further innovations in SSLB manufacturing technology. An in-depth understanding of the interactions between lasers and novel battery materials, such as halide- and sulfide-based solid electrolyte materials, will be key to improving the efficiency and applications of laser material processing. In general, laser material processing is expected to play a crucial role in the advancement of SSLB technologies, contributing to the development and manufacturing of safer, more efficient, and cost-effective SSLB solutions. While laser processing holds promise for processing SSLBs' materials and components to enhance their performance, more research and development are needed to better understand the laser material processes and to overcome the technological limitations so that it can be successfully implemented in the large-scale manufacturing of SSLBs. The advancements in SSLBs, enabled by laser material processing, could result in the development of more-efficient and longer-range electric vehicles and other portable electronic devices and contribute to a more sustainable future by reducing reliance on fossil fuels and promoting electric mobility.

Funding: This research received no external funding.

Acknowledgments: The author would like to thank the National Research Council of Canada for supporting this work.

Conflicts of Interest: The author declares no conflicts of interest.

Abbreviations

The following abbreviations are used in this manuscript:

SSLBs	Solid-state lithium batteries
PLD	Pulsed laser deposition
LLTO	Lithium lanthanum titanate
EVs	Electric vehicles
PEO	Poly(ethylene oxide)
LLZTO	$\text{Li}_{6.6}\text{La}_3\text{Zr}_{1.6}\text{Ta}_{0.4}\text{O}_{12}$
PEG	Poly(ethylene glycol)
VGCF	Vapor-grown carbon fiber
LCO	LiCoO_2
LLZO	$\text{Li}_7\text{La}_3\text{Zr}_2\text{O}_{12}$
R2R	Roll to roll
EIS	Electrochemical impedance spectroscopy
LiPON	Lithium phosphorous oxynitride

References

1. Yu, T.; Liu, Y.; Liu, Y.; Li, H.; Ning, W.; Feng, Y.; Zuo, D.; Zhou, H.; Guo, S. Intercepting dendrite growth with a heterogeneous solid electrolyte for long-life all-solid-state lithium metal batteries. *Small* **2024**, *20*, 2405446.
2. Khokhar, W.A.; Rafiq, M.-H.; Aleem, A.R.; Khokhar, D.A.; Ahmed, A.; Nazir, M.A.; Tufail, M.K. Recent Advancements in the Interfacial Stability of Garnet Solid Electrolytes and Design Strategies for Solid-State Lithium Batteries: A Review. *Energy Fuels* **2024**, *38*, 21674–21700.
3. Shi, C.; Takeuchi, S.; Alexander, G.V.; Hamann, T.; O'Neill, J.; Dura, J.A.; Wachsman, E.D. High Sulfur Loading and Capacity Retention in Bilayer Garnet Sulfurized-Polyacrylonitrile/Lithium-Metal Batteries with Gel Polymer Electrolytes. *Adv. Energy Mater.* **2023**, *13*, 2301656. [[CrossRef](#)]
4. Stramare, S.; Thangadurai, V.; Weppner, W. Lithium lanthanum titanates: A Review. *Chem. Mater.* **2003**, *15*, 3974–3990. [[CrossRef](#)]
5. Boaretto, N.; Garbayo, I.; Valiyaveettil-SobhanRaj, S.; Quintela, A.; Li, C.; Casas-Cabanas, M.; Aguesse, F. Lithium solid-state batteries: State-of-the-art and challenges for materials, interfaces and processing. *J. Power Sources* **2021**, *502*, 229919.
6. Huang, L.; Zhang, L.; Bi, J.; Liu, T.; Zhang, Y.; Liu, C.; Cui, J.; Su, Y.; Wu, B.; Wu, F. An Insight into Halide Solid-State Electrolytes: Progress and Modification Strategies. *Energy Mater. Adv.* **2024**, *4*, 0092.
7. López-Aranguren, P.; Reynaud, M.; Głuchowski, P.; Bustinza, A.; Galceran, M.; López del Amo, J.; Armand, M.M.; Casas-Cabanas, M. Crystalline LiPON as a Bulk-Type Solid Electrolyte. *ACS Energy Lett.* **2021**, *6*, 445–450.
8. Okumura, T.; Taminato, S.; Miyazaki, Y.; Kitamura, M.; Saito, T.; Takeuchi, T.; Kobayashi, H. LISICON-Based Amorphous Oxide for Bulk-Type All-Solid-State Lithium-Ion Battery. *ACS Appl. Energy Mater.* **2020**, *3*, 3220–3229. [[CrossRef](#)]
9. Hoff, L.C.; Scheld, W.S.; Vedder, C.; Stollenwerk, J. Laser sintering of ceramic-based solid-state battery materials. In Proceedings of the Laser-Based Micro- and Nanoprocessing XVI SPIE LASE, San Francisco, CA, USA, 22–27 January 2022.
10. Santomauro, A.; Huang, H.; Zou, M.; Ye, J.; Tong, J. Rapid laser reactive sintering of $\text{Li}_7\text{La}_3\text{Zr}_2\text{O}_{12}$ -based solid state battery electrolytes. *ECS Meet. Abstr.* **2021**, *240*, 1390. [[CrossRef](#)]
11. Hasani, A.; Luya, M.; Kamboj, N.; Nayak, C.; Joshi, S.; Salminen, A.; Goel, S.; Ganvir, A. Laser processing of liquid feedstock plasma-sprayed lithium titanium oxide solid-state-battery electrode. *Coating* **2024**, *14*, 224.
12. Wehbe, H.; Schmidt, L.O.; Kandula, M.W.; Dilger, K. Investigation of the effects of pulse width modulation on the laser sintering of LATP for all-solid-state batteries. *Appl. Phys. A* **2022**, *128*, 889. [[CrossRef](#)]
13. Kolb, D.; Reisacher, E.; Kreil, S.; Ruck, S.; Riegel, H.; Knoblauch, V. Microstructural investigations on selectively laser treated $\text{Li}_{6.6}\text{La}_3\text{Zr}_{1.6}\text{Ta}_{0.4}\text{O}_{12}$ solid electrolyte for solid-state batteries. *Microsc. Microanal.* **2023**, *29*, 1450–1451.
14. Lee, B.; Shin, S.; Kim, Y.; Han, J.T.; Jeong, B.; Park, J.H. Laser-assisted interfacial engineering for high-performance all-solid-state batteries. *ChemElectroChem* **2023**, *10*, e202300349.
15. Chen, L.; Li, Y.T.; Li, S.P.; Fan, L.Z.; Nan, C.W.; Goodenough, J.B. PEO/garnet composite electrolytes for solid-state lithium batteries. *Nano Energy* **2018**, *46*, 176–184. [[CrossRef](#)]
16. Zhang, Q.Q.; Liu, K.; Ding, F.; Liu, X.J. Recent advances in solid polymer electrolytes for lithium batteries. *Nano Res.* **2017**, *10*, 4139–4174. [[CrossRef](#)]
17. Su, Y.; Xu, F.; Qiu, Y.; Zhang, J.; Zhang, X.; Wang, H. Electrolyte based on laser-generated nano-garnet in poly(ethylene oxide) for solid-state lithium metal batteries. *Chem. Eng. J.* **2022**, *443*, 136418. [[CrossRef](#)]
18. Su, Y.; Mu, Z.; Qiu, Y.; Jiang, G.; Shenouda, A.; Zhang, X.; Xu, F.; Wang, H. Embedding of laser generated TiO_2 in poly(ethylene oxide) with boosted li + conduction for solid-state lithium metal batteries. *ACS Appl. Mater. Interfaces* **2023**, *15*, 55713–55722.
19. Chen, L.; Su, Y.; Zhang, J.; Zhang, H.; Fan, B.; Shao, G.; Zhong, M.; Wang, C.-A. Nanosecond laser cleaning method to reduce the surface inert layer and activate the garnet electrolyte for a solid-state li metal battery. *ACS Appl. Mater. Interfaces* **2021**, *13*, 37082–37090. [[CrossRef](#)]
20. Hördemann, C.; Anand, H.; Gillner, A. Ultrashort pulsed laser ablation for decapsulation of solid-state lithium-ion batteries. In Proceedings of the SPIE—The International Society for Optical Engineering, San Diego, CA, USA, 23 August 2017.
21. Wach, L.; Khaydarov, Y.; Garkusha, P.; Daub, R. Establishing laser cutting of components for sulfide-based solid-state batteries. *J. Laser Appl.* **2024**, *36*, 042026.
22. Yan, S.; Guo, D.; Yim, C.-H.; Merati, A.; Baranova, E.A.; Weck, A.; Abu-Lebdeh, Y. Cycling efficiency improvement of solid-state batteries-laser textured interfaces. *ECS Meet. Abstr.* **2023**, *243*, 1046.
23. Watanabe, T.; Gunji, T.; Suzuki, K.; Ando, N.; Nakamura, S.; Hayashi, N.; Soma, N.; Matsumoto, F. Application of a holed cathode and anode prepared with a picosecond pulsed laser for lithium-ion batteries—Performance of holed cathodes with solid-state electrolytes. *ECS Trans.* **2020**, *97*, 101–109.
24. Wu, S.; Zheng, H.; Zhang, N.; Cheng, W.; Liu, H.; Duan, H. Enhanced performance of flexible quasi-solid-state lithium batteries with high-loading cathode enabled by laser drilling. *J. Power Sources* **2022**, *542*, 231782.
25. Scheller, M.; Durdel, A.; Frank, A.; Jossen, A. Model-based performance evaluation of hybrid solid-state batteries: Impact of laser-ablated geometrical structures. *Batteries* **2024**, *10*, 392. [[CrossRef](#)]

26. Hille, L.; Oehler, A.; Chaja, M.; Zaeh, M.F. Scaling up picosecond laser ablation of a LATGP-type glass-ceramic solid electrolyte for all-solid-state battery production. *J. Manuf. Process.* **2023**, *106*, 188–201.
27. Yan, X.; Han, W. Ultrathin Garnet-Type Electrolytes, Solid Electrolytes for Advanced Applications. In *Solid Electrolytes for Advanced Applications Garnets and Competitors*; Springer International Publishing: Cham, Switzerland, 2020; pp. 155–166.
28. Saccoccio, M.; Yu, J.; Lu, Z.; Kwok, S.C.T.; Wang, J.; Yeung, K.K.; Yuen, M.M.F.; Ciucci, F. Low temperature pulsed laser deposition of garnet $\text{Li}_{6.4}\text{La}_3\text{Zr}_{1.4}\text{Ta}_{0.6}\text{O}_{12}$ films as all solid-state lithium battery electrolytes. *J. Power Sources* **2017**, *365*, 43–52.
29. Hanc, E.; Zajac, W.; Lu, L.; Yan, B.; Kotobuki, M.; Ziabka, M.; Molenda, J. On fabrication procedures of Li-ion conducting garnets. *J. Solid State Chem.* **2017**, *248*, 51–60.
30. Lee, J.Z.; Wang, Z.; Xin, H.L.; Wynn, T.A.; Meng, Y.S. Amorphous lithium lanthanum titanate for solid-state microbatteries. *J. Electrochem. Soc.* **2016**, *164*, A6268.
31. Aso, K.; Sakuda, A.; Hayashi, A.; Tatsumisago, M. All-Solid-State Lithium Secondary Batteries Using NiS-Carbon Fiber Composite Electrodes Coated with ($\text{Li}_2\text{S}-\text{P}_2\text{S}_5$) Solid Electrolytes by Pulsed Laser Deposition. *ACS Appl. Mater. Interfaces* **2013**, *5*, 686–690.
32. Sakuda, A.; Hayashi, A.; Ohtomo, T.; Hama, S.; Tatsumisago, M. All-solid-state lithium secondary batteries using LiCoO_2 particles with pulsed laser deposition coatings of ($\text{Li}_2\text{S}-\text{P}_2\text{S}_5$) solid electrolytes. *J. Power Sources* **2011**, *196*, 6735–6741.
33. Ito, Y.; Otoyama, M.; Ohtomo, T.; Hayashi, A.; Tatsumisago, M. Investigation of Structural Changes in Bulk-Type All-Solid-State Batteries using LiCoO_2 Particles with Sulfide Electrolyte Coatings. *ECS Meet. Abstr.* **2016**, *2016*, 262.
34. Sakurai, Y.; Sakuda, A.; Hayashi, A.; Tatsumisago, M. Preparation of amorphous $\text{Li}_4\text{SiO}_4-\text{Li}_3\text{PO}_4$ thin films by pulsed laser deposition for all-solid-state lithium secondary batteries. *Solid State Ion.* **2011**, *182*, 59–63.
35. Matsuyama, T.; Takano, R.; Tadanaga, K.; Hayashia, A.; Tatsumisago, M. Fabrication of all-solid-state lithium secondary batteries with amorphous TiS_4 positive electrodes and $\text{Li}_7\text{La}_3\text{Zr}_2\text{O}_{12}$ solid electrolytes. *Solid State Ion.* **2016**, *285*, 122–125.
36. Shiraki, S.; Oki, H.; Takagi, Y.; Suzuki, T.; Kumatai, A.; Shimizu, R.; Haruta, M.; Ohsawa, T.; Sato, Y.; Ikuhara, Y.; et al. Fabrication of all-solid-state battery using epitaxial LiCoO_2 thin films. *J. Power Sources* **2014**, *267*, 881–887.
37. Zheng, Y.; Hirayama, M.; Taminato, S.; Lee, S.; Oshima, Y.; Takayanagi, K.; Suzuki, K.; Kanno, R. Reversible lithium intercalation in a lithium-rich layered rocksalt Li_2RuO_3 cathode through a Li_3PO_4 solid electrolyte. *J. Power Sources* **2015**, *300*, 413–418.

Disclaimer/Publisher’s Note: The statements, opinions and data contained in all publications are solely those of the individual author(s) and contributor(s) and not of MDPI and/or the editor(s). MDPI and/or the editor(s) disclaim responsibility for any injury to people or property resulting from any ideas, methods, instructions or products referred to in the content.